The FEBS Journal

FEBS PRESS science publishing by scientists

A double point mutation at residues Ile14 and Val15 of Bcl-2 uncovers a role for the BH4 domain in both protein stability and function

Giovanni Monaco[1], Rita La Rovere[1], Spyridoula Karamanou[2], Kirsten Welkenhuyzen[1], Hristina Ivanova[1], Elien Vandermarliere[3], Marta Di Martile[4], Donatella Del Bufalo[4], Humbert De Smedt[1], Jan B. Parys[1], Anastassios Economou[2] and Geert Bultynck[1]

1 Laboratory of Molecular and Cellular Signaling, Department of Cellular and Molecular Medicine, Leuven Cancer Institute (LKI), KU Leuven, Belgium

2 Laboratory of Molecular Bacteriology, Department of Microbiology and Immunology, Rega Institute for Medical Research, KU Leuven, Belgium

3 Center for Medical Biotechnology, Department of Biochemistry, VIB-UGent, Ghent University, Belgium

4 Preclinical Models and New Therapeutic Agents Unit, Regina Elena National Cancer Institute, Rome, Italy

Keywords

apoptosis; Bcl-2-associated X protein; Bcl-2; Ca^{2+} signaling; hydrophobic core; inositol 1,4,5-trisphosphate receptor; point mutations; protein stability and turnover

Correspondence

G. Monaco and G. Bultynck, Laboratory of Molecular and Cellular Signaling, Department of Cellular and Molecular Medicine, Leuven Cancer Institute (LKI), KU Leuven, Campus Gasthuisberg, 3000 Leuven, Belgium

Fax: +32 16 330732

Tel: +32 16 330215

E-mails: giovanni.monaco@kuleuven.be (GM); geert.bultynck@kuleuven.be (GB)

(Received 19 December 2016, revised 30 September 2017, accepted 8 November 2017)

doi:10.1111/febs.14324

B-cell lymphoma 2 (Bcl-2) protein is the archetype apoptosis suppressor protein. The N-terminal Bcl-2-homology 4 (BH4) domain of Bcl-2 is required for the antiapoptotic function of this protein at the mitochondria and endoplasmic reticulum (ER). The involvement of the BH4 domain in Bcl-2′s antiapoptotic functions has been proposed based on Gly-based substitutions of the Ile14/Val15 amino acids, two hydrophobic residues located in the center of Bcl-2′s BH4 domain. Following this strategy, we recently showed that a BH4-domain-derived peptide in which Ile14 and Val15 have been replaced by Gly residues, was unable to dampen proapoptotic Ca^{2+}-release events from the ER. Here, we investigated the impact of these mutations on the overall structure, stability, and function of full-length Bcl-2 as a regulator of Ca^{2+} signaling and cell death. Our results indicate that full-length Bcl-2 Ile14Gly/Val15Gly, in contrast to wild-type Bcl-2, (a) displayed severely reduced structural stability and a shortened protein half-life; (b) failed to interact with Bcl-2-associated X protein (BAX), to inhibit the inositol 1,4,5-trisphosphate receptor (IP_3R) and to protect against Ca^{2+}-mediated apoptosis. We conclude that the hydrophobic face of Bcl-2′s BH4 domain (Ile14, Val15) is an important structural regulatory element by affecting protein stability and turnover, thereby likely reducing Bcl-2′s ability to modulate the function of its targets, like IP_3R and BAX. Therefore, Bcl-2 structure/function studies require pre-emptive and reliable determination of protein stability upon introduction of point mutations at the level of the BH4 domain.

Abbreviations

aa, amino acids; AUC, area under the curve; BAPTA, 1,2-Bis(2 aminophenoxy) ethane-N,N,N′,N′-tetraacetic acid; BAX, Bcl-2-associated X protein; Bcl, B-cell lymphoma; BH domain, Bcl-2 homology domain; Caspase, cysteine-dependent aspartate-specific protease; CD3, cluster of differentiation 3; ER, endoplasmic reticulum; GST, glutathione-*S*-transferase; HRP, horseradish peroxidase; IICR, IP_3-induced Ca^{2+} release; IP_3, inositol 1,4,5-trisphosphate; IP_3R, inositol 1,4,5-trisphosphate receptor; kDa, kiloDalton; Mcl-1, myeloid cell leukemia-1; MOMP, mitochondrial outer membrane permeabilization; PARP, poly-(ADP-ribose)-polymerase; PVDF, polyvinylidene fluoride; STS, staurosporine; TG, thapsigargin; UPR, unfolded protein response; VDAC, voltage-dependent anion channel; XBP1, x-box-binding protein 1.

Introduction

Apoptotic cell death is rigorously controlled by the intracellular ratio of anti- and pro-apoptotic B-cell lymphoma 2 (Bcl-2) proteins, a family of globular proteins acting upstream of mitochondrial outer membrane permeabilization (MOMP) and the cytosolic release of apoptogenic factors. Antiapoptotic Bcl-2 proteins, such as Bcl-2, B-cell lymphoma-extra large (Bcl-XL), and myeloid cell leukemia-1 (Mcl-1), guarantee cell survival mainly by neutralizing the pro-MOMP activity of their proapoptotic relatives [e.g., Bcl-2-associated X protein (BAX), Bcl-2 homologous antagonist killer (BAK)] at the mitochondria and by simultaneously restraining the flux of Ca^{2+} ions between endoplasmic reticulum (ER) and mitochondria [1–3]. Bcl-2 and its prosurvival relatives contain all four of the structurally conserved and functionally essential α-helical regions defined as Bcl-2-homology domains (BH; Fig. 1A,B, upper panel). The most N-terminal BH region, the BH4 domain, distinguishes these antiapoptotic proteins from some, but not all, of their proapoptotic counterparts [4,5]. Interestingly, recent studies revealed that the BH4 helix, either as isolated peptide [6–10], or as an integral part of full-length Bcl-2 [11–16] possesses an antiapoptotic activity separated from or additive to the one mediated by the other three BH domains (BH1-3). At the mitochondria, the BH4 domain of Bcl-2 prevents BAX activation [9]. At the ER, Bcl-2, via its BH4 domain, suppresses the shuttling of proapoptotic Ca^{2+} signals from ER to mitochondria by inhibiting the inositol 1,4,5-trisphosphate receptor (IP_3R), an ER-resident Ca^{2+}-release channel [17,18]. In the type 1 IP_3R (IP_3R1), the main binding site for Bcl-2 has been identified and pinpointed to a stretch of 20 amino acids (aa: 1389–1408 of mouse IP_3R1), located in the central modulatory domain of the IP_3R1 channel. As this amino acid sequence is largely conserved among the different IP_3R isoforms [18], the latter inhibitory mechanism is considered a common denominator among IP_3R1, IP_3R2, and IP_3R3 channels. On the Bcl-2 side of the interaction, we reported that at least four surface-accessible residues in the BH4 domain, Lys17, His20, Tyr21, and Arg26 (Fig. 1B, cyan bold and [18]), coordinate Bcl-2′s inhibitory function on the IP_3Rs. Moreover, the positively charged residue Lys17 is a key determinant for this functional interaction, although a Lys17Asp full-length mutant of Bcl-2 shows residual protection against Ca^{2+}-mediated apoptosis, underpinning the relevance of the other residues for this process. Irrespective of the specific function of Bcl-2 at the mitochondria or ER, other studies have conducted similar mutational analysis in order to map the residues of the BH4 domain essential for Bcl-2 antiapoptotic function. Based on glycine substitutions, these reports identified six indispensable residues (Ile14, Val15, Tyr18, Ile19, Lys22, Leu23) whose mutations completely abolished the protective function of Bcl-2 [16,19–22]. However, most of these residues are poorly surface accessible since they are part of the putative hydrophobic face of the BH4 helix that docks this region inside the globular nucleus of Bcl-2 [9,23] (Fig. 1A, lower panel). Particularly, Ile14 and Val15 constitute the core of the hydrophobic binding interface and are embedded in the α-helical backbone of BH4. More recently, we and others showed that short α-helical BH4 peptides carrying amino acidic substitutions at Ile14 and/or Val15, failed to protect against apoptosis [9,10]. Both investigations attributed the impaired peptide function to a disruption of the minimal α-helical structure of $BH4_{Bcl\text{-}2}$ necessary for interaction with BAX [9] and IP_3Rs [10]. However, the structural role of this hydrophobic core, comprising residues Ile14 and Val15, has not yet been elucidated in the context of full-length Bcl-2.

Here, we studied whether Ile14 and Val15 were critical for the overall stability of Bcl-2, independently or additively to a possible local effect on the BH4 moiety. Therefore, we evaluated the activity and stability of wild-type Bcl-2 versus a Bcl-2 mutant carrying two glycine substitutions at Ile14 and Val15 (hereafter Bcl-2 IV/GG). The Bcl-2 IV/GG was compared to another BH4 domain mutant, Bcl-2 Lys17Asp (hereafter Bcl-2 K/D), which according to our previous analysis [18] affects Bcl-2 activity without impairing its structural integrity. We investigated the mutated versions of Bcl-2 in a series of *in silico* and *in vitro* experiments assessing the antiapoptotic activity of these mutants in relation to their thermodynamic stability, their protein turnover and their BAX or IP_3R1-binding and inhibiting properties.

Results

Mutations at residues Ile14 and Val15 impact Bcl-2 protein function

The 3D structure of the Bcl-2 protein with its four BH domains is presented in Fig. 1A, including a close-up of the BH4 domain highlighting residues Ile14, Val15, and Lys17 relevant for this work. First, we used the highly reliable screening for nonacceptable polymorphisms 2 (SNAP2) method [24] to determine the likelihood for Bcl-2-N-terminal (aa: 1–30) mutations (see 3D in Fig. 1A and linear sequences in Fig. 1B) to influence the function of the human protein (UniProt Kb: P10415-1) and possibly contribute to human

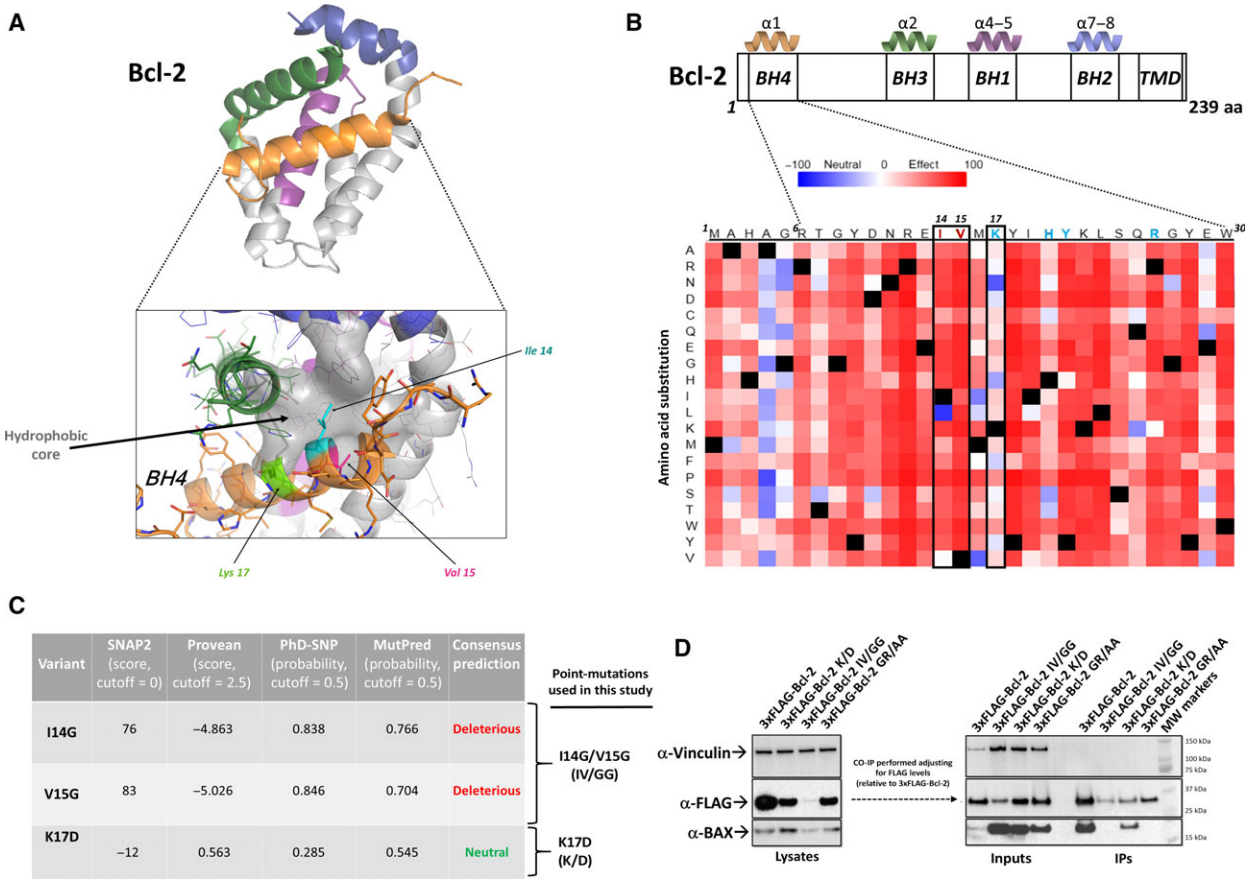

Variant	SNAP2 (score, cutoff = 0)	Provean (score, cutoff = 2.5)	PhD-SNP (probability, cutoff = 0.5)	MutPred (probability, cutoff = 0.5)	Consensus prediction	Point-mutations used in this study
I14G	76	−4.863	0.838	0.766	Deleterious	I14G/V15G (IV/GG)
V15G	83	−5.026	0.846	0.704	Deleterious	
K17D	−12	0.563	0.285	0.285	Neutral	K17D (K/D)

Fig. 1. Substitution of residues 14 and 15 of Bcl-2's BH4 domain severely impacts Bcl-2 function. (A, top) Unique three-dimensional structural features in Bcl-2 protein with the depicted location of its α-helical BH domains. Orange = BH4; Green = BH3; Purple = BH1 and Blue = BH2. PDB-entry 4LXD [74]. (A, bottom) Zoom-in on the hydrophobic core that locks Ile14 and Val14 but not the surface-accessible Lys17. (B, top) Linear representation of the key structural features of the human Bcl-2 protein (BH domains and transmembrane domain). Color code for the BH helices as in (A). Helix number is assigned to each BH domain according to the Uniprot entry P10415. (B, bottom) SNAP2 mutability landscape for Bcl-2's N-terminal fragment from residue 1 to residue 30 which contains the BH4 domain. The heat map shows the predictions for the effects of all 19 non-native variants (*y*-axis) on protein function. SNAP2 score ranges from the most neutral (−100, blue) to the strongest effect (+100, red). The rectangular boxes highlight the results for aa Ile14, Val15, and Lys17. Ile14 and Val15 are also highlighted in red to differentiate them from the four nearby residues involved in IP_3R1 interaction, which are depicted in cyan. (C, table) Consensus results obtained by using five different on-line tools for prediction of the specific impact of Ile14Gly, Val15Gly, and Lys17Asp point mutations on Bcl-2 biological function. Predictive tools employed: SNAP2, scores above 0 indicate a deleterious effect on protein function; PROVEAN, scores below −2.5 indicate a deleterious effect on protein function; PhD-SNP, probability above 0.5 indicates a deleterious effect on protein function; MutPred, probability above 0.5 indicates a deleterious effect on protein function (C, right) Nomenclature used for the mutant investigated in this study (Ile14Gly-Val15Gly, IV/GG) or the mutant used as control (Lys17Asp, K/D). (D) FLAG pull-down assays were performed to assess the BAX-binding properties of 3xFLAG-Bcl-2, 3xFLAG-Bcl-2 K/D or 3xFLAG-Bcl-2 IV/GG, overexpressed in COS-1 cells. The left blot shows the steady-state expression levels. The right blot shows the inputs from the adjusted samples to obtain similar amounts of the various FLAG-tagged Bcl-2 proteins in the pull-down experiments using agarose beads coupled to a FLAG-recognizing antibody. The hydrophobic cleft defective version of Bcl-2 (3xFLAG-Bcl-2 GR/AA), which fails to bind BAX, was used as negative control. Immunoblots were stained with an anti-Bax antibody (bottom), an anti-FLAG-HRP-conjugated antibody (middle) to stain Flag-tagged proteins or an anti-Vinculin antibody (top) to stain vinculin (loading control). Results shown are representative of at least three independent experiments with similar results.

diseases (see Materials and methods for details). This systematic *in silico* analysis yielded a comprehensive protein mutability landscape for $BH4_{Bcl\text{-}2}$. As shown by the relative heat map (Fig. 1B, lower panel), point mutations targeting the hydrophobic residues Ile14 and/or Val15 are very likely to disrupt Bcl-2 function (scores higher than 0, red color scheme) in comparison with the relatively neutral profile resulting from substitutions at Lys17. Our next approach consisted in predicting the effects of the specific IV/GG dicodon mutation on the biological function of Bcl-2 and comparing these results to the ones obtained for the

well-characterized mutation K17D [18]. For this purpose, we used, besides SNAP2, three additional independent predictive tools based on an evolutionary conservation algorithm (Protein Variation Effect Analyzer-PROVEAN, [25]), on an evolutionary conservation and structure homology algorithm (Mutpred, [26]) or on a SNAP2-like machine learning algorithm Predictor of human Deleterious Single-Nucleotide Polymorphisms (PhD-SNP, [27]; see provided references for further methodological details). These methods derived a broad consensus as to the potential impact of the IV/GG or K/D substitutions on protein function (Fig. 1C). Both the Ile14Gly and the Ile15Gly substitutions are predicted to be deleterious to Bcl-2 function in contrast to the relatively neutral effect produced by the K/D variant (Fig. 1C).

To validate our prediction analysis, we compared the ability of Bcl-2 and the two mutants derivatives (K/D and IV/GG) to heterodimerize with the proapoptotic protein BAX. Therefore, we transiently transfected COS-1 cells with 3xFLAG-Bcl-2, 3xFLAG-Bcl-2 K/D, and 3xFLAG-Bcl-2 IV/GG in order to perform a pull-down with anti-FLAG and to look for the co-immunoprecipitated BAX. We adjusted the amount of lysates used for each IP condition in order to compensate for the lower expression levels of the 3xFLAG-Bcl-2-mutants, especially for 3xFLAG-Bcl-2 IV/GG, whose steady-state expression levels are very low (see Fig. 1D, left panel). The 3xFLAG-Bcl-2 GR/AA mutation (Gly145Ala and Arg146Ala) was used as a negative control for this interaction, since this mutant is characterized by a structurally disrupted hydrophobic cleft (BH3-BH1-BH2; [28–30]). Similarly to 3xFLAG-Bcl-2 GR/AA, 3xFLAG-Bcl-2 IV/GG failed to interact with BAX, while 3xFLAG-Bcl2 K/D mutant remained able to bind BAX (Fig. 1D, right panel).

These initial results already indicate that the IV/GG dicodon mutation may severely impact Bcl-2 protein function, while the effect of the K/D mutation is expected to be moderate.

Bcl-2 IV/GG is severely impaired in binding IP_3R, inhibiting IP_3R-induced Ca^{2+} release and protecting against Ca^{2+}-dependent apoptosis

To further translate the *in silico* predictions toward the actual function of Bcl-2, we initially focused on the characterization of the IP_3R-binding properties of Bcl-2 IV/GG protein. We performed glutathione-*S*-transferase (GST) pull-down assays, using cell lysates from COS-1 cells overexpressing 3xFLAG-Bcl-2 or 3xFLAG-Bcl-2 IV/GG. These lysates were incubated with GST-Domain 3, purified from bacteria, that corresponds to a major part of the regulatory domain of IP_3R1 [31] and contains the previously described Bcl-2-binding site on IP_3R [32]. SDS/PAGE analysis showed that in contrast to the wild-type protein, the 3xFLAG-Bcl-2 IV/GG is severely impaired in binding to GST-Domain 3 (Fig. 2A). To evaluate the functional significance of the above results, we compared the inhibitory function of 3xFLAG-Bcl-2 and 3xFLAG-Bcl-2 IV/GG on IP_3R1-mediated Ca^{2+} release by performing single-cell Ca^{2+} measurements using Fura-2. COS-1 cells were transiently transfected with 3xFLAG-vector (empty vector), 3xFLAG-Bcl-2, or 3xFLAG-Bcl-2 IV/GG and an m-Cherry-expressing plasmid at a 3 : 1 ratio to visualize transfected cells. Only mCherry-positive cells were included in the measurements. For each recording, we first chelated the free extracellular Ca^{2+} using 5 mM 1,2-Bis(2 aminophenoxy) ethane-N,N,N′,N′-tetraacetic acid (BAPTA) in order to measure Ca^{2+} released exclusively from the ER. Sixty seconds after BAPTA addition, we monitored the Ca^{2+} signals of ~ 10–15 cells per condition/experiment in response to 1 μM ATP, an extracellular agonist that elicits IP_3R-mediated Ca^{2+} signaling. In contrast to 3xFLAG-Bcl-2, which reduced the ATP-induced [Ca^{2+}] peak, 3xFLAG-Bcl-2 IV/GG did not significantly affect this amplitude (Fig. 2B,C). Next, we examined the effect of the IV/GG substitution on the antiapoptotic function of Bcl-2. To this end, we treated COS-1 cells overexpressing 3xFLAG-vector, 3xFLAG-Bcl-2 or 3xFLAG-Bcl-2 IV/GG with staurosporine (1 μM STS 6 h) and compared the extent of the cysteine-dependent aspartate-specific protease (caspase)-dependent cleavage of poly-(ADP-ribose)-polymerase (PARP). As previously reported [18], after 6 h of treatment with 1 μM STS, 3xFLAG-Bcl-2-overexpressing cells displayed significantly reduced PARP cleavage compared to the control cells. In contrast, 3xFLAG-Bcl-2 IV/GG overexpression could not protect the cells against STS-induced apoptosis (Fig. 2D,E and raw data in Fig. S1). These findings are in line with our previous data, which showed that the Bcl-2-BH4-IV/GG peptide lost its antiapoptotic effect [10].

To corroborate these results in a more cell physiological context, we used microplate reader recordings of WEHI7.2 cells that stably express Bcl-2 or Bcl-2 IV/GG. We followed Ca^{2+} release in response to a high concentration (10 $\mu g \cdot mL^{-1}$) of anticluster of differentiation 3 (CD3), which triggers strong T-cell receptor (TCR) activation and subsequent IP_3R-mediated Ca^{2+} release [33]. Compared to native WEHI7.2 cells, which display no detectable levels of Bcl-2 (Fig. 3A), WEHI7.2 cells expressing wild-type Bcl-2 displayed a significant decrease in anti-CD3-induced Ca^{2+} release.

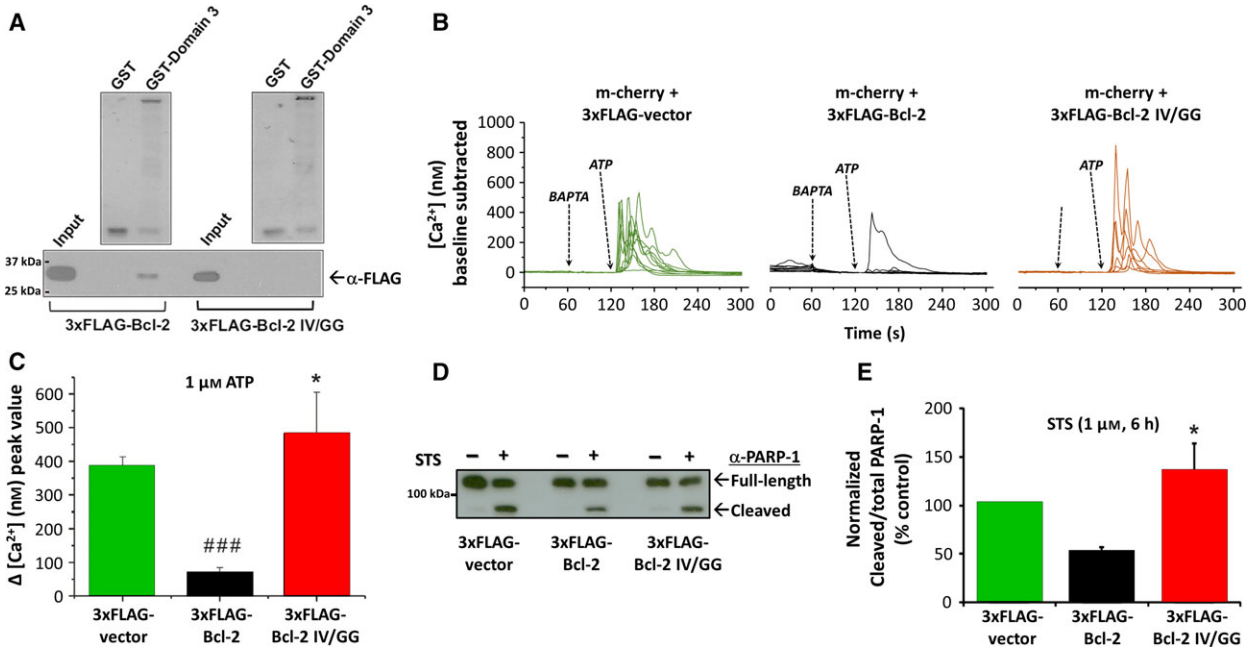

Fig. 2. Bcl-2 IV/GG fails to interact with the IP_3R, to reduce IP_3 induced Calcium release (IICR) and to protect against STS-induced cell death in transiently transfected COS-1 cells. (A) GST pull-down assays were used to assess the binding of 3xFLAG-Bcl-2 or 3xFLAG-Bcl-2 IV/GG, expressed in COS-1 cells, to either GST or GST-Domain 3, the latter being part of the central regulatory domain of the IP_3R. The GST-tagged proteins were incubated with COS-1 lysates, adjusted to yield comparable levels of the FLAG-tagged proteins, and pulled down using glutathione-Sepharose beads. Samples were analyzed via SDS/PAGE for total protein detection (GelCode blue, top) and western blotting for FLAG-tag detection (anti-FLAG-HRP-conjugated antibody, bottom). Results shown are representative of three independent experiments with similar results ($n = 3$). (B) Representative traces, obtained from 10 to 15 Fura-2-loaded COS-1 cells, showing the cytosolic $[Ca^{2+}]$ rises in response to ATP (1 μM, added after 120 s) after extracellular free Ca^{2+} has been chelated with BAPTA (5 mM, added after 60 s). Fluorescent signals of Fura-2 (F340/F380) were only monitored in cells coexpressing the mCherry plasmid. Signals were: (a) calibrated to obtain $[Ca^{2+}]$ (nM) values and (b) subtracted to baseline. A total of ~ 80 cells per transfection condition were analyzed on three different experimental days. Each line on the graph corresponds to the Ca^{2+} signal obtained from a single cell over time. The different lines represent the individual cells simultaneously measured in one well. ATP was applied as an agonist to assess IP_3R-mediated Ca^{2+} release, whereby the peak $[Ca^{2+}]$ was quantified in each cell. (C) Quantitative analysis of the amplitude of the ATP-induced Ca^{2+} signals in mCherry-expressing COS-1 cells transfected with the different FLAG vectors. Data points represent mean ± SEM calculated from three independent experiments. ###3xFLAG-Bcl-2 is statistically different from 3xFLAG-vector ($P < 0.001$; one-way ANOVA, $P = 0.0002$). *3xFLAG-Bcl-2 IV/GG is statistically different from 3xFLAG-Bcl-2 (one-way ANOVA, $P = 0.0326$). (D) Western blot analysis using anti-PARP-1 antibody for monitoring PARP-1 cleavage upon STS treatment (1 μM for 6 h) in 3xFLAG-vector, 3xFLAG-Bcl-2 and 3xFLAG-Bcl-2 IV/GG-expressing COS-1 cells. (E) Quantification of the ratio between the immunoreactive bands of the cleaved over the total PARP in the different transfected COS-1 cell populations from three independent experiments. The ratio of cleaved over total PARP obtained for control cells was set at 100% and the other ratios were normalized to this value. Error bars are representative of the mean ± SEM obtained from the three independent experiments. *3xFLAG-Bcl-2 IV/GG is statistically different from 3xFLAG-Bcl-2 (*T* test, $P = 0.04533$).

As indicated by the representative traces (Fig. 3B) and their quantification (Fig. 3C), cells expressing Bcl-2 IV/GG displayed a similar response to that of the control cells. The differences in the anti-CD3-induced Ca^{2+} rises were not due to differences in the initial Ca^{2+} content in the ER, as neither Bcl-2 nor Bcl-2 IV/GG overexpression affected the ER Ca^{2+}-store content measured after thapsigargin (TG) application, which is in line with previous reports [18,34] (Fig. 3D). Finally, the viability of WEHI7.2 cells was examined to further evaluate the residual antiapoptotic function of Bcl-2 IV/GG. WEHI7.2 control cells and WEHI7.2 cells expressing either Bcl-2 or Bcl-2 IV/GG were treated with STS (1 μM in DMSO) or DMSO alone for 6 h and examined by the Trypan blue exclusion assay. While Bcl-2-expressing cells showed a ~ 50% reduction in dye uptake and therefore in death index, Bcl-2 IV/GG expression failed to protect the WEHI7.2 cells against cell death (Fig. 3E).

Altogether, these biological results demonstrate that altering IV into GG in full-length Bcl-2 has a deleterious impact on Bcl-2′s functional properties (Figs 2 and 3).

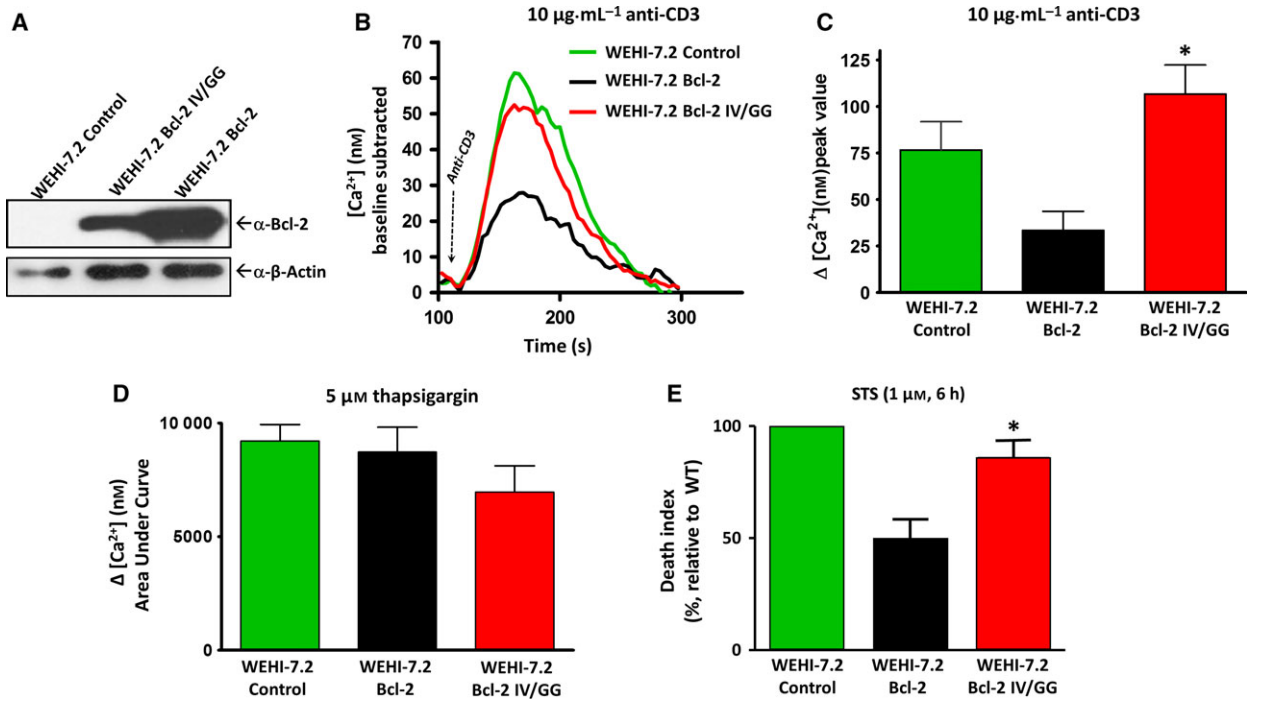

Fig. 3. Bcl-2 IV/GG fails to reduce IICR and to protect against STS-induced apoptosis in stably transfected WEHI7.2 cell lines. (A) WEHI-7.2 cell lines with a stable expression of Bcl-2 or Bcl-2 IV/GG were created. The expression levels of Bcl-2 and Bcl-2 IV/GG were examined by western blotting analysis using an anti-Bcl-2 antibody. Control WEHI-7.2 cells display no detectable levels of endogenous Bcl-2. (B) Representative Ca^{2+} traces recording the Ca^{2+} elevation induced by 10 $\mu g \cdot mL^{-1}$ anti-CD3 antibody in WEHI-7.2 cells, WEHI-7.2 cells expressing Bcl-2 or WEHI7.2 cells expressing Bcl-2 IV/GG. EGTA (1 mM) was added 60 s after recording was started and anti-CD3 was added 60 s after EGTA addition. Traces were obtained for cell populations measured on a Flexstation microplate reader. (C) Quantitative analysis of the amplitude of the anti-CD3-induced Ca^{2+} signals for the three different WEHI-7.2 cell lines. All experiments were repeated independently three times and data points represent mean ± SEM. The results obtained for WEHI-7.2 Bcl-2 IV/GG are statistically different (*) from the ones of WEHI-7.2-Bcl-2 (*T* test, $P = 0.0225$). (D) Quantitative analysis of the AUC of the TG (5 µM)-induced Ca^{2+} responses in control, Bcl-2 expressing- or Bcl-2 IV/GG-expressing WEHI-7.2 cell lines. Bars are representative of the mean ± SEM obtained from three independent experiments. (E) Quantitative analysis from three independent experiments of the STS-induced cell death normalized to the values obtained for the control WEHI7.2 cells (% relative to WT). Bars are representative of the mean ± SEM. The death index was determined by the difference between the Trypan blue-positive fraction of STS-treated cells and the DMSO-treated cells: $(\text{Trypan blue-positive})_{STS} - (\text{Tryphan blue-positive})_{DMSO}$. Results for WEHI-7.2-Bcl-2 IV/GG are statistically different (*) from the ones obtained for WEHI-7.2-Bcl-2 (*T* test, $P = 0.0484$).

Recombinant Bcl-2 IV/GG shows a severe decrease in overall protein stability

We previously showed that the IV/GG mutation carried on an isolated $BH4_{Bcl\text{-}2}$ peptide (aa: 6–30) destabilized the α-helical structure of the native $BH4_{Bcl\text{-}2}$ peptide [10]. To address this local effect in the full-length Bcl-2 (human Bcl-2, UniProt Kb: P10415-1), the structural organization of the IV/GG mutant was initially evaluated *in silico* by using the I-TASSER (http://zhanglab.ccmb.med.umich.edu/I-TASSER/; [35]) and the Phyre2 (http://www.sbg.bio.ic.ac.uk/phyre2; [36]) structural modeling servers.

For each of the mutants, the top three structural models obtained from I-TASSER (Fig. 4A, top 3D structures) and Phyre2 predictions (Fig. 4A, bottom panels) displayed excellent structural alignment with Bcl-2 [see also RMSD < 0.5 Angstroms (Å)]. This suggests that neither the Bcl-2 IV/GG nor the comprehensively characterized Bcl-2 K/D substitutions [18] affect the local secondary structure of the $BH4_{Bcl\text{-}2}$. Additionally, we averaged the 3D-structures of the three most-representative Bcl-2-IV/GG models and exploited them to better examine the potential spatial organization of the BH4-domain residues previously proposed to be important for IP_3R interaction (Lys17, His20, Tyr21, and Arg26 [18]). The analysis suggested no drastic spatial rearrangement of these 4 residues' side chains in the IV/GG mutant versus the native protein, although small fluctuations no > 7 Å were predicted for Arg26 (Fig. 4B). We therefore examined the effects

of the IV/GG substitution on the overall structure of Bcl-2 by comparing the *in silico* thermodynamic stability of Bcl-2 IV/GG and Bcl-2 K/D variants (see Materials and methods for methodological details). A highly destabilizing effect of the Bcl-2 IV/GG substitution was predicted by all five tools employed (Fold-X [37], Eris [38], CC/PBSA [39], I-mutant 2.0 [40], Duet [41]) with calculated $\Delta\Delta G$ values above 4 kcal·mol^{-1} (Fig. 4C). On the contrary, Bcl-2 K/D was predicted to have a relatively stable protein structure with $\Delta\Delta G$ values ≤ 1 kcal·mol^{-1} (Fig. 4C). To directly test the effect of the introduced mutations on the structural stability of Bcl-2, we bacterially purified the three proteins and performed a CD spectral analysis (Fig. 4D). Wavelength scan analysis in the far-UV resulted in characteristic spectra of an extensively α-helical protein, with minima at 208 and 221 nm, for 6xHis-Bcl-2 (Fig. 4D, black curve). The same was true for the K/D derivative, although its total helical content was reduced, suggesting some structural alteration (Fig. 4D, blue curve). In contrast, 6xHis-Bcl-2 IV/GG showed extensive loss of helical content, consistent with extensive structural alteration (Fig. 4D, red curve). To further corroborate this analysis, we collected CD spectra at 222 nm during thermal gradients and determined the apparent melting temperatures (Tm_{app}) of the proteins as a direct indicator of their thermal stability (Fig. 4E). A detailed view of the CD spectra obtained for 6xHis-Bcl-2, 6xHis-Bcl-2 IV/GG, and 6xHis-Bcl-2 K/D at different temperatures is presented in Fig. S2. 6xHis-Bcl-2 was found to be very stable with a Tm_{app} of 76 °C (Fig. 4E, black curve), while the K/D mutant appears to be less stable than the wild-type, visible as faster loss in its helical structure at increasing temperatures (Tm_{app} of 46.3 °C; Fig. 4E, blue curve). For 6xHis-Bcl-2 IV/GG, no Tm_{app} could be determined, which indicates that the protein is already completely destabilized even at low temperatures (Fig. 4E, red curve). Next, since there is a proven positive correlation between protein stability, protein folding, and resistance to proteolysis [42–44], we assessed whether bacterially expressed 6xHis-tagged Bcl-2 IV/GG would be predominantly directed into the insoluble inclusion bodies fraction. The resultant immunoblots showed that most of the 6xHis-Bcl-2 IV/GG protein almost completely accumulated in the insoluble fraction, with no apparent intact protein visible in the soluble fraction at short blot exposures (Fig. 4F). The 6xHis-Bcl-2 K/D protein was mostly present in the soluble supernatant similarly to the native protein (Fig. 4F), however, a small portion appeared in the insoluble fraction. This finding may relate to the increased susceptibility of the Bcl-2 K/D protein to unfolding, discovered in the thermal gradient CD analysis using the purified proteins.

These data indicate that both mutations introduced in Bcl-2 have structural consequences on the stability of the protein. Mutation of Ile14Val15 into Gly14Gly15 results in a completely destabilized, unfolded protein, while the Lys17Asp mutation only mildly destabilizes the Bcl-2 protein. Thus, these results imply that BH4 is an important structural element that stabilizes Bcl-2 structure.

Cellular 3xFLAG-Bcl-2 IV/GG is subject to rapid turnover mostly driven by the proteasome

Finally, we examined the overall structural stability and turnover of human Bcl-2 IV/GG in the more suitable mammalian expression systems represented by COS-1 and WEHI7.2 cells, where endogenous protein folding and proper post-translational modifications are guaranteed [45]. Expression levels of Bcl-2 IV/GG in mammalian cell lines appeared to be low (Fig. 1D, left panel and 3A). Accordingly, the steady-state expression of Bcl-2 IV/GG was consistently lower than that of Bcl-2 K/D or of the native Bcl-2 in WEHI7.2 cells passaged 20–30 times in selective medium (Fig. 5A), and in COS-1 cells immunoblotted 12–48 h post-transfection (Fig. 5B for representative blot, Fig. 5C for the quantification). The steady-state protein levels are determined by the rate of synthesis and degradation; therefore, we investigated the effective cellular stability of Bcl-2 IV/GG in chase experiments using the protein synthesis inhibitor cycloheximide (CHX; Fig. 5D for representative blots, Fig. 5E for the quantification). COS-1 cells were transiently transfected with 3xFLAG-Bcl-2, 3xFLAG-Bcl-2 IV/GG, or 3xFLAG-Bcl-2 K/D and then treated with the protein synthesis inhibitor CHX (20 μg·mL^{-1}) and a pan-caspase inhibitor (Z-VAD-FMK, 4 μM) to warrant cell viability. The levels of 3xFLAG-proteins were monitored by immunobloting, which revealed that 3xFLAG-Bcl-2 IV/GG was very rapidly degraded in ~ 30 min similarly to what was observed for the endogenous short-lived protein Mcl-1 (Fig. 5D,E and [46,47]). In contrast, both 3xFLAG-Bcl-2 and 3xFLAG-Bcl-2 K/D remained abundant upon increased exposure time to CHX with very similar half-life values (26–28 h, Fig. 5E). In addition, we assessed whether Bcl-2 IV/GG expression was sufficient to cause ER stress and activate the unfolded protein response (UPR). For this, we monitored the unconventional splicing of the mRNA encoding the transcriptional factor X-Box-binding protein-1 (XBP1) [48,49]. Transfection of COS-1 cells with each of the 3xFLAG vectors (3xFLAG-Bcl-2, 3xFLAG-Bcl-2 IV/GG, 3xFLAG-Bcl-2 K/D, or 3xFLAG-Vector)

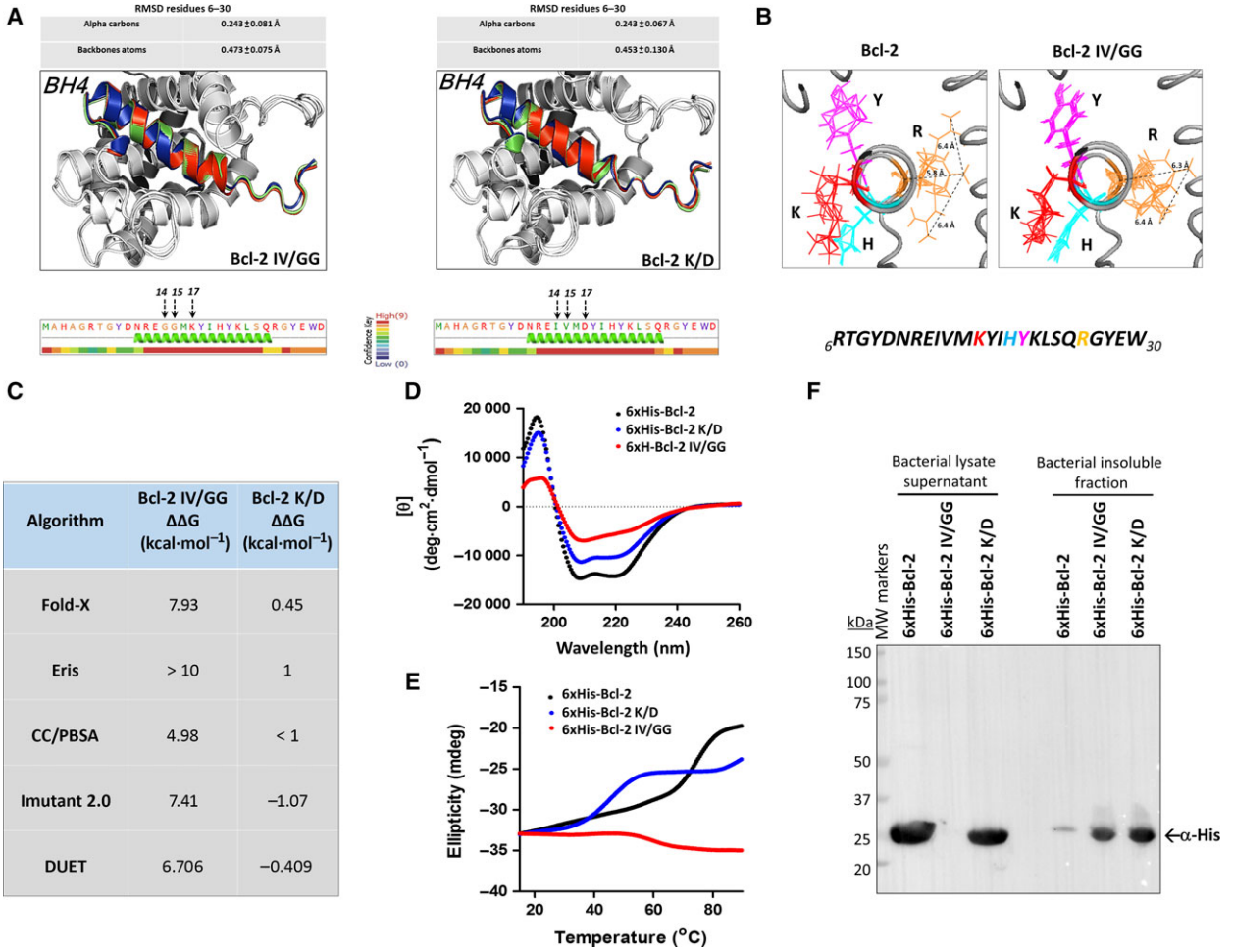

Fig. 4. While its BH4-α-helical motif is likely preserved, Bcl-2 IV/GG displays overall structural instability *in silico* and as bacterially purified protein. (A, top) The amino acid sequences corresponding to the Bcl-2 IV/GG (left) and Bcl-2 K/D (right) substitutions were submitted to the I-TASSER v 2.1 prediction server and the resulting best three PDB models were structurally aligned using the molecular visualization system PyMOL. The secondary structure of the BH4 domain is highlighted in color. The green, red, and blue colors depict, respectively, the first, second, and third PDB model for each of the mutants in order of prediction accuracy. RMSD of atomic positions between the 6–30 amino acidic region of WT and mutant's models is also reported in the above table. (A, bottom). Secondary structure predictions of Bcl-2 IV/GG (left) and Bcl-2 K/D (right) using the protein homology/analogy recognition Engine version 2 (Phyre[2]). The sequence has been processed to predict the locations of α-helices. The confidence in the predicted state for each position is shown using a rainbow color code: red = high confidence, blue = low confidence. (B) Zoom-in on the primary structure of the BH4 domain of Bcl-2 and Bcl-2 IV/GG. The side chains of the key residues involved in IP_3R regulation are depicted in color. The trajectories for the best three predictive models of Bcl-2 or Bcl-2 IV/GG, obtained as in (A), were averaged and the resulting 3D-structure was visualized in PyMOL. (C) Calculation of free energy changes between wild-type and each of the mutant proteins (I14G/V15G or K17D) using five different prediction methods to estimate protein thermodynamic stability: highly destabilizing mutations ($\Delta\Delta G > 3$ kcal·mol^{-1}) or neutral mutations ($-1 < \Delta\Delta G < 1$ kcal·mol^{-1}). (D) Far-UV CD spectra of Bcl-2 and mutant derivatives. These bacterial purified Bcl-2 variants are devoid of their C-terminal- transmembrane tail (pET47-Bcl-2 Δ23). Experiments, carried out at 15 °C (10 μM; 250 μL; 5 mM MOPS, pH: 7.5; 5 mM NaCl), were normalized for protein concentration; (θ): molar ellipticity. The differences seen are attributed to the effect of the mutations on the helical content of Bcl-2 ($n = 3$). Representative spectra are shown following smoothing (5FFT). (E) Thermal denaturation curves (15–85 °C) obtained by monitoring ellipticity at 222 nm, by far-UV CD, while heating the protein samples (10 μM; 250 μL; 5 mM MOPS, pH: 7.5; 5 mM NaCl) at 1 °C·min^{-1} ($n = 3$). A representative experiment is shown following smoothing (15FFT) and normalization of all curves at the first data point. (F) Representative western blot showing the relative amount of bacterial expressed 6xHis-Bcl-2, 6xHis-Bcl-2 IV/GG, and 6xHis-Bcl-2 K/D that are soluble (left) or aggregated in inclusion bodies (right). Equal volumes of lysate supernatant (left lanes) or sarkosyl-extracted (right lanes) fractions have been loaded on the gel. The arrowhead indicates the band corresponding to the His antibody staining.

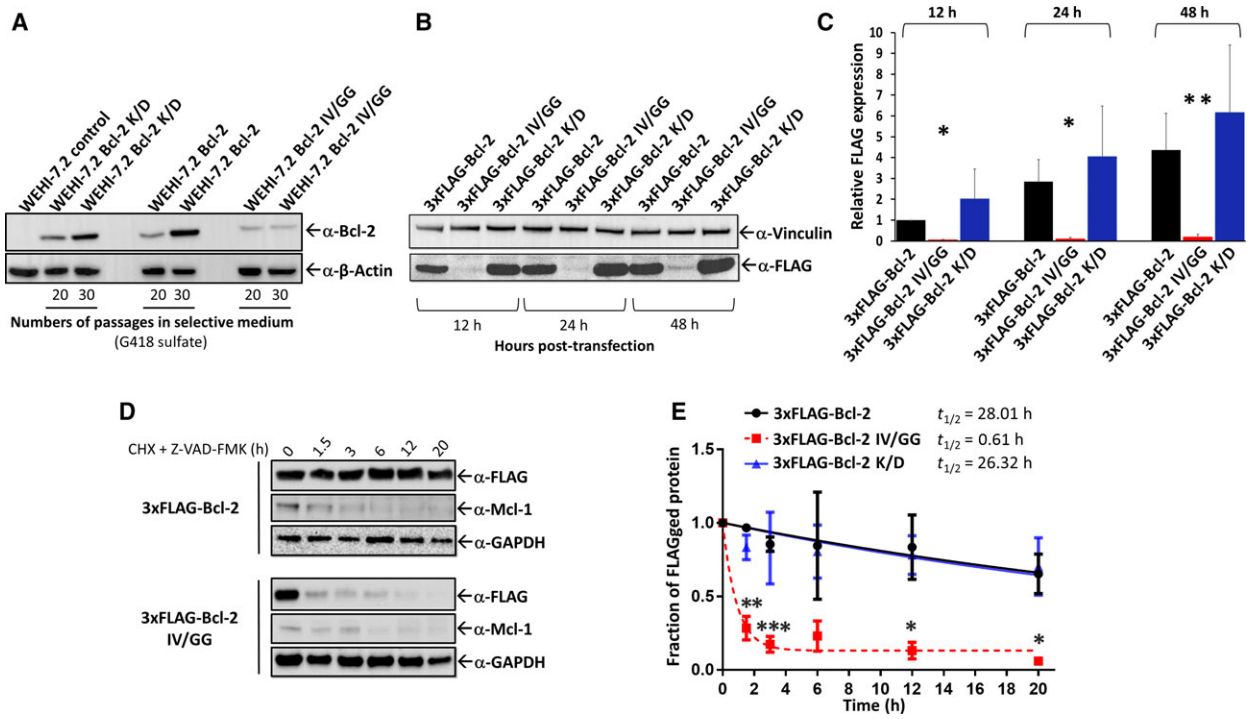

Fig. 5. Bcl-2 IV/GG displays lower steady-state levels than wild-type Bcl-2 due to its reduced half-life. (A) Stable WEHI-7.2 transfectants (Control, Bcl-2, Bcl-2 K/D, and Bcl-2 IV/GG) were cultured in selective conditions (G418 sulfate, 1 mg·mL^{-1} growth medium) and lyzed after 20 or 30 passages. Lysates were subjected to SDS/PAGE/immunoblotting using Bcl-2 antibody (top) or β-actin antibody (bottom). (B) Representative blot of transient COS-1 transfectants (3xFLAG-Bcl-2, 3xFLAG-Bcl-2 IV/GG, 3xFLAG-Bcl-2 K/D) lyzed 12 h, 24 h or 48 h after transfection and subjected to SDS/PAGE/immunoblotting using an anti-FLAG-HRP-conjugated antibody. (C) Quantification of the FLAG immunoreactive signals (3xFLAG-Bcl-2, 3xFLAG-Bcl-2 IV/GG, and 3xFLAG-Bcl-2 K/D) obtained for four independent transfection time courses. FLAG-tag was quantified by densitometry as band intensity ratio relative to 3xFLAG-Bcl-2 at 12 h, which was set at 1. Bars are representative of the mean ± SEM.*3xFLAG-Bcl-2 IV/GG is statistically different from 3xFLAG-Bcl-2 and 3xFLAG-Bcl-2 K/D (one-way Anova, Friedman test, $P_{12\ h}$ = 0.0417; $P_{24\ h}$ = 0.0407; $P_{48\ h}$ = 0.0046). (D) COS-1 cells transfected with 3xFLAG-Bcl-2 or the 3xFLAG-Bcl-2 IV/GG vector for 48 h were treated with CHX (final concentration 20 μg·mL^{-1}) and the pan-caspase inhibitor Z-VAD-FMK (final concentration 4 μM) for the indicated time and subjected to SDS/PAGE/immunoblotting using an anti-FLAG-HRP-conjugated antibody, an antibody against the short-living protein Mcl-1 and an antibody against GAPDH (loading control). The exposure times have been adjusted to better compare FLAG-tagged-protein half-lives. (E) Quantitative analysis of 3xFLAG-Bcl-2, 3xFLAG-Bcl-2 IV/GG, and 3xFLAG-Bcl-2 K/D half-lives ($t_{1/2}$) derived from three separate CHX-chase experiments. FLAG-tag was quantified by densitometry as band intensity ratio relative to time 0 h, which was set at 1. The intensity data were fit to one-phase exponential-decay to estimate the degradation rate constant, which then was used to calculate a half-life ($t_{1/2}$). Data points are representative of the mean ± SEM. Results for the time points 1.5, 3, 12, and 20 h of 3xFLAG-Bcl-2 are statistically different (*) from the ones obtained for 3xFLAG-Bcl-2 IV/GG (*T* test, $P_{1.5\ h}$ = 0.0062; $P_{3\ h}$ = 6.04E-05; $P_{12\ h}$ = 0.0495; $P_{20\ h}$ = 0.0305). **Statistically significant differences were considered at $P < 0.01$. ***Statistically significant differences were considered at $P < 0.001$.

slightly increased XBP1 splicing, only indicating a minimal UPR activation (Fig. 6A) after transfection. TG, a well-recognized inducer of ER stress and thus of UPR [50], served as a positive control in these tests. Finally, we examined the degradation pathways responsible for 3xFLAG-Bcl-2 IV/GG turnover by performing a CHX-chase experiment (6 h) in the presence of the proteasomal inhibitor MG132 (20 μM), the lysosome inhibitor E64D (5 μM) or the ER-associated degradation (ERAD) inhibitor eeyarestatin I (EerI, 100 nM). Only proteasomal inhibition was able to partially restore the 3xFLAG-Bcl-2 IV/GG-protein levels in the CHX/Z-VAD-FMK treated samples (Fig. 6B,C). The short-living protein Mcl-1, known to be degraded through the proteasome [51], was taken as an internal control.

These results suggest that an overall structural destabilization of Bcl-2 IV/GG leads to its rapid proteasomal turnover and underlies the observed functional defects.

Discussion

The major finding of this study is that the BH4 domain's hydrophobic core formed by residues Ile14

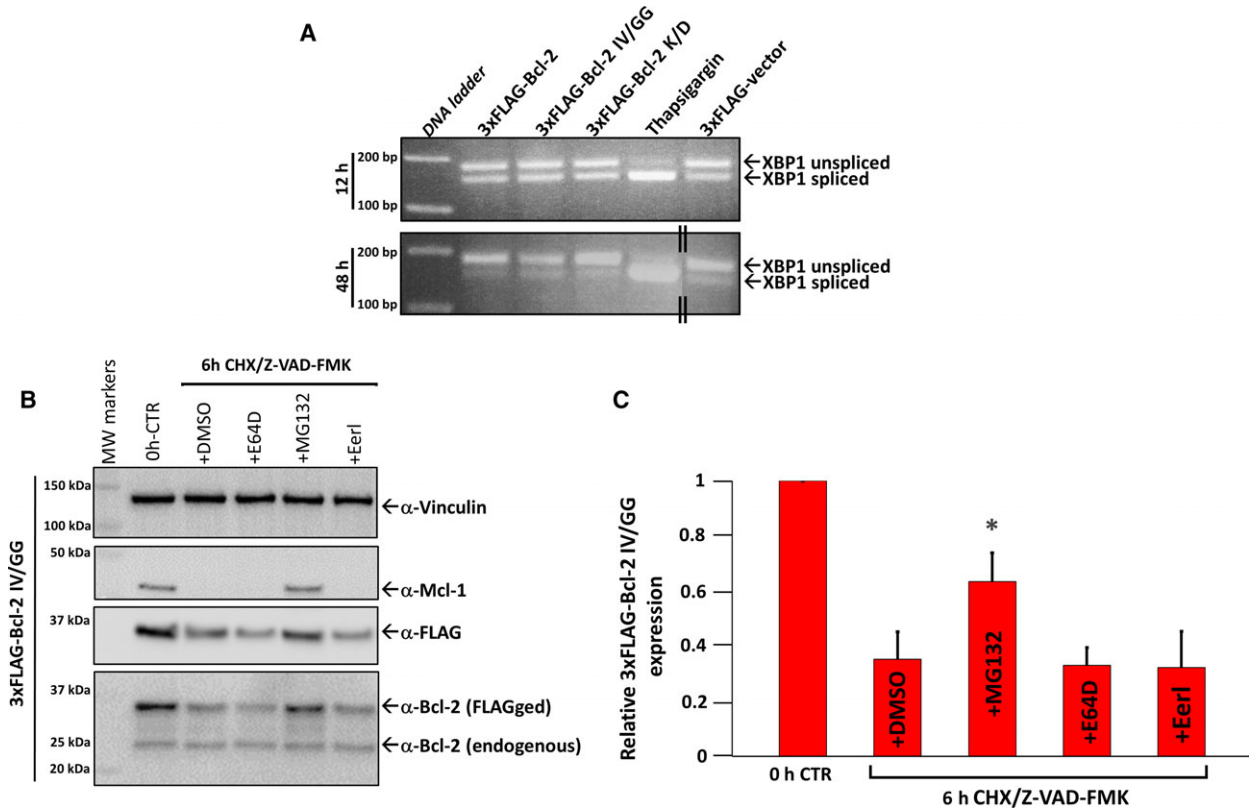

Fig. 6. The rapid degradation of Bcl-2 IV/GG is mainly mediated by the proteasome. (A) 12 h (top) or 48 h (bottom) post-transfection COS-1 cells expressing 3xFLAG-Bcl-2, 3xFLAG-Bcl-2 IV/GG, 3xFLAG-Bcl-2 K/D or 3xFLAG-vector were evaluated for XBP-1 splicing. XBP1 cDNA was amplified by RT PCR and subjected to agarose gel electrophoresis. The lengths of DNA size markers (200 and 100 bp) are shown on the left of the gel while the spliced and unspliced variants of XBP-1 are indicated on the right by arrowheads. TG-treated cells (5 μM, 3 h, were used as positive control for XBP1 splicing. (B) 3xFLAG-Bcl-2 IV/GG transfectants underwent a CHX-chase experiment (6 h incubation) in the presence of the proteasomal inhibitor MG132 (20 μM), the lysosome inhibitor E64D (5 μM) or the ERAD inhibitor Eerl (100 nM). The total cell lysates were immunoblotted with Mcl-1, FLAG, Bcl-2, and Vinculin antibodies. The signal obtained with latter antibody was used as loading control. Representative western blots from three experiments ($n = 3$) are shown. (C) Quantitative analysis of the CHX experiment shown in B. FLAG-tag was quantified by densitometry as band intensity ratio relative to time 0 h (untreated control), which was set at 1. Bars are representative of the mean ± SEM. The 3xFLAG-Bcl-2 IV/GG densitometric measurements are statistically different between the samples cotreated with MG132 and the DMSO (vehicle)-treated samples (*, one-way Anova, Bonferroni adjustment, $P = 0.0108$).

and Val15 is critical for Bcl-2-protein stability and function. Glycyl substitution of these residues, a strategy previously employed to attribute survival functions to the BH4 domain [16,19–23], strongly impairs the overall structural stability of the protein, resulting in a major decrease of Bcl-2′s half-life.

The BH4 domain is important for the biological functions of Bcl-2 and Bcl-XL in counteracting apoptosis [11,13,52–56], promoting angiogenesis [55], suppressing autophagy [57], sustaining bio-energetics [58] and controlling Ca^{2+}-flux systems, like IP_3Rs [17], ryanodine receptors (RyRs) [59] and Bax Inhibitor-1 [60] in a variety of cellular, physiological and pathophysiological systems and models. Bcl-2 truncated of its BH4 domain turns into a proapoptotic protein through exposure of its BH3 domain and/or activation of Bax/Bak-dependent MOMP [14,15,61], while deleting this domain in Bcl-XL impaired its interaction with IP_3R3 and its ability to support bio-energetics [58]. The BH4 domain is not only necessary for the antiapoptotic function of Bcl-2/Bcl-XL, it is by itself also sufficient to protect cells against apoptosis. For instance, loading cells with a $BH4_{Bcl\text{-}2}$-derived peptide via electroporation, protects cells against cell death induced by Ca^{2+}-dependent stimuli, including cytochrome *c* and STS [7,8,11]. This can be largely attributed to the ability of $BH4_{Bcl\text{-}2}$ to directly bind to and inhibit IP_3R channels and to the ability of $BH4_{Bcl\text{-}XL}$ to directly bind to and inhibit voltage-dependent anion channel 1 (VDAC1) channels, thereby preventing the transfer of proapoptotic Ca^{2+}-signals from the ER Ca^{2+} stores to the mitochondria [18,56]. More

recently, it has been shown that $BH4_{Bcl\text{-}2}$ domain could also directly target BAX and prevent BAX activation, thereby protecting against BAX-mediated apoptosis [9]. The latter study used an elegant approach based on chemical stapling of a BH4 domain-like peptide to favor an α-helical formation, and showed that the regulation of Bax by $BH4_{Bcl\text{-}2}$ was critically dependent on its α-helical properties. Also, IP_3R regulation by $BH4_{Bcl\text{-}2}$ was dependent on its α-helical properties, since alterations in the BH4-domain-peptide sequence that decreased its propensity to form an α-helix resulted in impaired IP_3R binding and inhibition [10].

However, the functional impact of such alterations in the BH4 domain has not yet been assessed at the level of full-length Bcl-2. Furthermore, one of these alterations, namely Ile14Val15 into Gly14Gly15 (IV/GG), has been extensively used in a number of studies to determine the involvement of $BH4_{Bcl\text{-}2}$ in the regulation of certain molecular processes or cellular targets [16,19–23]. Using a series of *in silico* predictions, *in vitro* binding and *in cellulo* functional Ca^{2+}-signaling and apoptosis approaches, we found that changing IV into GG led to a dysfunctional Bcl-2 protein (Figs 1, 2 and 3). This mutant failed to interact with and inhibit IP_3R channels (Figs 2A–C and 3A–C) as well as with the main proapoptotic protein BAX (Fig. 1D). Although this result is somewhat expected as these same alterations in the isolated $BH4_{Bcl\text{-}2}$ sequence abolished the IP_3R- and BAX-regulatory properties of the BH4 peptide, the underlying reasons for this appeared to be less obvious in the full-length protein. Indeed, residue substitutions may disrupt the biological function and cellular effects of a certain protein not only by directly changing the 'active' residues/binding site but also by affecting the overall structure of the protein, a property often overlooked. The change of protein scaffolding may eventually affect protein stability [62,63], particularly because the globular conformation of proteins is predominately stabilized by hydrophobic interactions [64,65]. In agreement with this, Bcl-2 IV/GG was highly unstable after *in silico*, bacterial expression and CD analyses (Fig. 4C–E). Thus, this N-terminal Bcl-2 mutant might be more susceptible to misfolding, thereby causing the rapid turnover and degradation observed *in cellulo* (Fig. 5A–D). Instead, Bcl-2 K/D, which is only partially structurally unstable displayed wild-type-like protein half-life (Fig. 5A–D), conserved its ability to bind Bax (Fig. 1D) and partially protected against apoptosis (figs 7 and 8 of our previous publication [18]). The tertiary structure of Bcl-2 reveals evident reasons for the strong deleterious effect of replacing I14V15 into G14G15, since stability of the globular structure of Bcl-2 is likely dependent on docking of the BH4 helix in the cradle formed by the other proximal BH helices and their hydrophobic residues (see Fig. 1A). Consequently, our data further indicate that results based on BH4 mutations, especially those affecting the hydrophobic-core residues, must be interpreted with great caution before implying the direct involvement of $BH4_{Bcl\text{-}2}$ in the regulation of specific molecular processes or targets.

Importantly, a recent, elegant study [66] showed that the stability of a given Bcl-2-family member is the main factor contributing to its antiapoptotic effect in leukemic cells. Indeed, Bcl-2, Bcl-XL, or Bcl-W were, due to their superior stability, more effective in protecting leukemic cells against anticancer drugs than the less stable Bcl-B, Bfl-1, or Mcl-1. Expression of Bcl-B, Bfl-1, or Mcl-1 at similar levels as Bcl-2, Bcl-XL, or Bcl-w resulted in equally potent protection against anticancer drugs, independently of their selective interaction with proapoptotic family members. This shows that the structural stability of Bcl-2-family members is a key feature underpinning their antiapoptotic potency in cells. Another hint for the contribution of $BH4_{Bcl\text{-}2}$ to the structural stability of Bcl-2 has been recently provided by the work of Han *et al.* [67]. This study identified a compound, BDA-366, that selectively binds the $BH4_{Bcl\text{-}2}$ with very high affinity. BDA-366 binding to Bcl-2 actually switched this protein from an anti-apoptotic into a proapoptotic protein that directly activates BAX through the exposure of its BH3 domain. This may indicate that BDA-366, by binding the BH4 domain, disturbs intramolecular interactions essential for maintaining the proper Bcl-2 structure, possibly those between BH4 and BH3 domain.

In our experiments, overexpression of 3xFLAG-Bcl-2 IV/GG did not result in spontaneous cell death (Fig. 2D), but appeared to sensitize cells to cell death-inducing agents like STS (Fig. 2E). Moreover, the levels of IP_3-induced Ca^{2+} release (IICR) appeared slightly higher than in cells transfected with the empty vector (Fig. 2B,C). Therefore, we cannot exclude that Bcl-2 IV/GG is intrinsically toxic to cells, but we postulate that toxicity is mostly avoided by the rapid turnover of the Bcl-2 IV/GG mutant protein. Somewhat unexpectedly, expression of the highly unstable Bcl-2 IV/GG did not induce a marked UPR response ([68,69]; Fig. 6A). Nonetheless, results from Fig. 6B,C show that 3xFLAG-Bcl-2 IV/GG degradation is mostly rescued by the co-incubation of the CHX-treated cells with the proteasome inhibitor MG132. On the contrary, the lysosomal and ERAD inhibitors, E64D and EerI, respectively, were unable to restore 3xFLAG-Bcl-2 IV/GG levels. The latter data suggest that 3xFLAG-Bcl-2 IV/GG escapes ER quality control and

is rapidly degraded by the proteasome, likely not engaging the lysosomal/autophagy pathway [70], as previously suggested for Bcl-2 lacking its BH4 domain [57].

In conclusion, the overall structural stability of Bcl-2 is critically dependent on the presence of V14I15 in the center of its BH4 domain and of Bcl-2 hydrophobic nucleus, affecting Bcl-2′s ability to bind/counteract BAX and IP_3R activities and in turn to protect against apoptosis. Notably, the present results further provide a rationale for 1) distinguishing local from overall effects on Bcl-2 structure following BH4 domain mutagenesis, and 2) targeting Bcl-2 prosurvival function in cancer by weakening one of Bcl-2 stability hotspots represented by the BH4 domain.

Materials and methods

In silico predictive analysis

To pre-emptively evaluate the impact of each point mutation on Bcl-2 function, we used four web tools based on different prediction algorithms: SNAP2 (https://rostlab.org/services/snap/), PROVEAN (http://provean.jcvi.org/seq_submit.php), Mutpred (http://mutpred.mutdb.org/), and PhD-SNP (http://snps.biofold.org/phd-snp/phd-snp.html). The predictive algorithm of SNAP2 is based on a learning device method known as neural network. SNAP2 is trained on (a) a set of ~ 100.000 mutations whose molecular and experimental effect is annotated in the Protein Mutant Database (PMD) and SWISSPROT and (b) all human disease-causing mutations contained in the Online Mendelian Inheritance in Man (OMIM) and the human variation (HumVar) datasets. For a given substitution, SNAP2 predicts a score that ranges from −100 (strongly neutral) to +100 (strongly impacting protein function/disease-like). The default score threshold of PROVEAN is set at −2.5 and values lower than −2.5 indicate a deleterious mutation. The output of MutPred and PhD-SNP contains the probability that the amino acid substitution is deleterious and disease-associated.

To calculate the change in pseudo-thermodynamic stability induced by the Ile14Gly/Val15G or the Lys17Asp substitution, we used five automated estimators of free energy change variations ($\Delta\Delta G$). In more detail, the thermodynamic stability of a protein is determined by the difference in Gibbs free energy (ΔG) between the folded and the unfolded states. Thus, the variations in free energy change ($\Delta\Delta G$) between the native and mutant protein are as read-out for identifying potential stabilizing or destabilizing point mutations. $\Delta\Delta G$ values > 1 kcal·mol^{-1} are considered representative of a structure-destabilizing mutation, while values < 1 kcal·mol^{-1} are indicative of neutral or stabilizing mutations. These thermodynamic predictive tools rely on: (a) physical-based potential (PBP) approaches, which seek to recapitulate the forces felt by a protein in solution; (b) knowledge-based potential (KBP) approaches, which are obtained from a statistical analysis of empirical information extracted from protein databases; (c) various combination of the previous two approaches (for detailed explanation see provided references or link for each *in silico* tool). Four of the used estimators are accessible online on their respective webservers: Eris (http://dokhlab.unc.edu/tools/eris/), CC/PBSA (http://www.biotechnik.nat.uni-erlangen.de/research/boeckmann/cc-pbsa.shtml), I-mutant 2.0 (http://folding.biofold.org/i-mutant/i-mutant2.0.html) and DUET (http://bleoberis.bioc.cam.ac.uk/duet/stability). The 5th automated estimator, Fold-X, was used as an executable downloaded from http://foldxsuite.crg.eu/.

For both the above predictive approaches, the query protein sequence was provided in FASTA format obtained from the Universal Protein Resource (UniProt Kb: P10415-1). Alternatively, we used the I-TASSER v 2.1 webserver (http://zhanglab.ccmb.med.umich.edu/I-TASSER/) to obtain the 3D-structure of the query protein before predicting the functional and stability impact of the examined amino acidic substitution. I-TASSER builds protein models using iterative assembling procedures and multiple threading alignments from template structure libraries. The accuracy of the I-TASSER prediction is estimated by the confidence score. In the case of our Bcl-2 K/D and IV/GG mutants, the three most accurate I-TASSER models for each mutant were downloaded as protein data bank (PDB) file and imported in PyMOL, a molecular graphics software (http://www.pymol.org).

To estimate the integrity of the BH4 secondary structure, we aligned in PyMOL these three I-TASSER models for each mutant and calculated with the SUPERPOSE software (http://wishart.biology.ualberta.ca/SuperPose/, [71]) the relative RMSD in relation to the native BH4 domain (aa: 6–30) structure. We further averaged the 3D-structure of each set of models to obtain information about the local spatial organization of the BH4-domain-residues previously proposed to be important for the IP_3R interaction (Lys17, His20, Tyr21 and Arg26, [18]). We employed the PyMOL measurement wizard to measure the spatial fluctuations involving those residues in the IV/GG versus the wild-type Bcl-2 protein.

Plasmids and PCR site-directed mutagenesis

The prokaryotic expression vector pGEX-6p2 (Amersham Biosciences, GE Healthcare, Diegem, Belgium) encoding aa 923–1581 of mouse IP_3R1 (Domain 3) fused to a GST protein (GST-Domain 3) was obtained as previously described [32]. The prokaryotic expression vector pET47-Bcl-2 Δ23, for bacterial expression and purification of a C-terminal truncated 6-His-tagged Bcl-2, was kindly provided by V. Shoshan-Barmatz (Department of Life Sciences, Ben-Gurion University of the Negev, Israel).

The eukaryotic expression vector 3xFLAG-Bcl-2 was generated by subcloning the respective full-length cDNAs into p3xFLAG-myc-CMV-24 vector (Sigma-Aldrich, Munich, Germany) at *Hin*dIII/*Bgl*II sites. The eukaryotic expression vectors pSFFV-Neo and pSFFV-Neo-Bcl-2, used for stable transfection, were kindly provided by C. W. Distelhorst (Case Western Reserve University, Cleveland, USA).

The 3xFLAG-Bcl-2 K/D, IV/GG mutants were generated by PCR site-directed mutagenesis of the 3xFLAG-Bcl-2 or for the corresponding mutants of the pET47-Bcl-2 Δ23 vector. The following primers were used: K/D forward (5′-GATAACCGGGAGATAGTGATGGATTACATCCATTATAAGCTGTCG-3′); K/D reverse (5′-CGACAGCTTATAATGGATGTAATCCATCACTATCTCCCGGTTATC-3′); IV/GG forward (5′-CGGGGTACGATAACCGGGAGGGAGGGATGAAGTACATCCATTATA-3′); IV/GG reverse 5′-TATAATGGATGTACTTCATCCCTCCCTCCCGGTTATCGTACCCCG-3′). For 3xFLAG-Bcl-2 GR/AA double mutant, we used the same primers as in [26]: GR/AA forward (5′-ATCCCCATGGCAGCAGTAGATCAAGCGCTGAGGGAGGCA-3′); GR/AA reverse (5′-TGCCTCCCTCAGCGCTTGATCTACTGCTGCCATGGGGAT-3′).

The pSFFV-Neo-Bcl-2 IV/GG vector was also obtained by PCR site-directed mutagenesis. To introduce the desired point mutations, we designed and used the following primers: Neo-Bcl-2 IV/GG forward (5′-CGGGGTACGACAACCGGGAGGGAGGGATGAAGTACATCCATTATA -3′); Neo-Bcl-2 IV/GG reverse (5′- TATAATGGATGTACTTCATCCCTCCCTCCCGGTTGTCGTACCCCG- 3′).

All constructs were verified by sequencing (Agowa AG, Berlin, Germany).

Cell culture and transfections

COS-1 cells were seeded at a density of 15 000 cells·cm^{-2} and cultured in Dulbecco's modified Eagle's medium (DMEM) supplemented with 10% FBS (Sigma-Aldrich) at 37 °C, 10% CO_2. At 2 days after plating, COS-1 cells were transiently transfected with the empty p3xFLAG-Myc-CMV-24 vector (Sigma-Aldrich) or with this vector containing the cDNA of Bcl-2, the Bcl-2 IV/GG mutant or the Bcl-2 K/D mutant. The transfection procedure was performed using JetPRIME transfection reagent (Polyplus Transfections, New York, NY, USA) following the manufacturer's recommendations. For Ca^{2+}-imaging experiments, COS-1 cells were also cotransfected with a pcDNA 3.1-mCherry vector (Invitrogen, Carlsbad, CA, USA) using a DNA ratio of 1 : 3 between pcDNA 3.1-mCherry and p3xFLAG-Myc-CMV-24 vectors.

WEHI7.2 murine cells were grown as described previously [32] and nucleofected with pSFFV-Neo, pSFFV-Neo-Bcl-2, or pSFFV-Neo-Bcl-2 IV/GG vectors, using the Amaxa nucleofector and the dedicated Mouse T-cell Nucleofector Kit according to the manufacturer's instructions (Amaxa-Lonza AG, Basel, Switzerland). Subsequently, resistant cells were stably selected with 1 mg·mL^{-1} G418 (Invitrogen) as described [72] without performing clonal expansion.

FLAG-co-immunoprecipitation assay

COS-1 cells overexpressing the 3xFLAG-Bcl-2 wt, 3xFLAG-Bcl-2 K/D, 3xFLAG-Bcl-2 IV/GG, or 3xFLAG-Bcl-2 GR/AA were harvested and lyzed in a buffer containing 25 mM Hepes, pH 7.5, 1% Triton X-100, 10% glycerol, 0.3 M NaCl, 1.5 mM $MgCl_2$, 1 mM DTT, 2 mM EDTA, 2 mM EGTA and protease inhibitor cocktail tablets (Roche, Basel, Switzerland). 100 μg of lysate were mixed with 30 μL anti-DYKDDDDK-tag conjugated resin (Biolegend, San Diego, CA, USA) in the lysis buffer in total volume of 400 μL. The samples were incubated for 2.5 h using a head-over-head rotor at 4 °C. The beads were washed two times with washing buffer (50 mM Tris-HCl (pH 8.0), 150 mM NaCl, 1% NP-40, 0.5% sodium deoxycholate and 0.1% SDS) via centrifugation for 1 min at 3000 ***g*** using spin columns. The FLAG-complexes were eluted by competitive incubation with the Anti-DYKDDDDK-tag peptide (10 μg, dissolved in 50 mM Tris-HCl and 150 mM NaCl) for 30 min at 15 °C. After further centrifugation (1 min at 500 ***g***), 25 μL of LDS supplemented with 1 : 200 β-mercaptoethanol was added to the resulting eluates. Fifteen microliter of each sample was subjected to western blot analysis as described below in 'Western-blot analysis and antibodies' and incubated with the appropriate primary antibody.

Recombinant protein expression and purification

BL21 (DE3) Escherichia coli cells were transformed with pGEX-6p2 or pET47b+ constructs for expression of GST and GST-Domain 3 or of the different 6xHis-tagged versions of human Bcl-2-Δ23, respectively. The expressed GST-tagged proteins were purified as previously described [18]. For 6xHis-Bcl-2, 6xHis-Bcl-2 IV/GG, and 6xHis-Bcl-2 K/D, BL21 (DE3) bacteria were grown overnight at 37 °C, diluted to an A600 of 0.2, exposed to a heat shock of 40 °C for 2 h, followed by induction of protein expression with isopropyl-D-1-thiogalactopyranoside for 120 min at 20 °C. Bacteria were lyzed in lysis buffer (150 mM NaCl, 10 mM Tris pH 7.4, 20% glycerol, 30 mM Imidazole) by sonication and subsequently centrifuged (40.000 × ***g*** for 40 min). The insoluble debris was resuspended in 27 mL 1% sarkosyl (*N*-lauroylsarcosine)/PBS, incubated on ice for 30 min, centrifuged (13.000 × ***g*** at 4 °C for 10 min) and adjusted to a Triton X-100 final concentration of 2%. Both the soluble and detergent solubilized fractions underwent western blot analysis. The 6xHis-tagged proteins contained in the soluble fraction were further purified by using a nickel-nitrilotriacetic acid resin (Ni-NTA agarose) and eluted from the resin using 500 mM imidazole.

All fusion proteins were dialyzed against standard PBS without added Ca^{2+} or Mg^{2+} (2.67 mM KCl, 1.47 mM KH_2PO_4, 137.93 mM NaCl, 8.06 mM Na_2HPO_4; Invitrogen) using Slide-A-Lyzer with a cutoff of 3 kiloDalton (kDa; Thermo Fisher Scientific, Pittsburg, PA, USA). After dialysis, the concentration of the purified proteins was determined using BCA Protein Assay Reagent (Thermo Fisher Scientific), and the quality and integrity were examined by SDS/PAGE and GelCode blue stain reagent (Thermo Fisher Scientific) before downstream analyses.

CD experiments

CD spectra were recorded using a Jasco J-1500 spectropolarimeter (Oklahoma City, OK, USA) equipped with a Peltier element for temperature control and a six-position cuvette holder. Proteins were dialyzed in 5 mM MOPS pH:7.5; 5 mM NaCl, for 15 h, at 4 °C; 3× changes; constant stirring. Aggregated material was removed by centrifugation (20 000 ***g***; 15 min; 4 °C) before protein concentration was determined on a Nanodrop instrument (280 nm; 2000 series; Thermo). The molecular extinction coefficient and molecular weight for A280 analysis was determined using the Expasy server (http://web.expasy.org/protparam/). Wavelength scan measurements (190–260 nm) were performed with 5–20 μM protein, at 15 °C; in 5 mM MOPS pH 7.5; 5 mM NaCl, using 1 mm quartz cuvettes (Hellma, Müllheim, Germany); data pitch: 0.5 nm; bandwidth: 1 nm; scanning speed: 50 $nm \cdot min^{-1}$; DIT: 0.5 s; accumulation: 3. Variable temperature measurements (15–85 °C) were performed with 5–10 μM protein; in 5 mM MOPS pH 7.5; 5 mM NaCl, using 1 mm quartz cuvettes (Hellma); interval 0.5 °C; gradient 1 $°C \cdot min^{-1}$; DIT:0.5 s; bandwidth: 1 nm. Wavelength (190–260 nm) and temperature (15–85 °C) scan measurements were carried out with 5 μM protein; in 5 mM MOPS pH 7.5; 5 mM NaCl, using 1 mm cuvettes (Hellma); data interval 5 °C; temperature gradient 1 $°C \cdot min^{-1}$; DIT: 1 s; bandwidth: 1 nm. Data were analyzed using the SPECTRA ANALYSIS v.2 software (Jasco); Tm_{app} were derived by acquiring the first derivatives of the melting curves, using the calculus function of ORIGIN7 (GE).

GST pull-downs

Equal amounts (30 μg) of the intact full-length GST-fusion proteins or parental GST (control) were incubated in interaction buffer (50 mM Tris-HCl, 300 mM NaCl, 1 mM EDTA, 1% NP-40, 0.5% sodium deoxycholate, 0.5% BSA and protease inhibitor cocktail (complete Mini, EDTA-free, Roche, 1 tablet/10 mL), pH 7.0) with 200 μg of cleared lysate from COS-1 cells transiently transfected with the 3xFLAG-Bcl-2 vector, 3xFLAG-Bcl-2 K/D, 3xFLAG-Bcl-2 IV/GG, or the empty vector. COS-1 lysates have been adjusted to yield comparable levels of the FLAG-tagged proteins. Glutathione-Sepharose 4B beads (GE Healthcare Europe GmbH, Munich, Germany) were immediately added to the protein mix before incubation continued in a head-over-head rotator for 2 h at 4 °C. The beads were washed four times with modified Interaction Buffer (150 mM NaCl instead of 300 mM NaCl, without BSA), and complexed GST-fusion proteins were eluted by incubating the beads with 40 μL LDS (Invitrogen) for 3 min at 95 °C and collected after centrifuging at 500 ***g*** for 5 min. Eluates (10 μL) were subjected to western blot (see section below 'Western-blot analysis and antibodies') and incubated with the appropriate primary antibody.

CHX-chase assay

Forty-eight hours post-transfection with the 3xFLAG-Bcl-2 vector, 3xFLAG-Bcl-2 K/D, 3xFLAG-Bcl-2 IV/GG or the empty vector, COS-1 cells were incubated with 10% FBS DMEM containing 20 $\mu g \cdot mL^{-1}$ CHX (Sigma) and the Pan-Caspase Inhibitor Z-VAD-FMK (4 μM; R&D systems, Minneapolis, MN, USA). Additionally, the proteasome inhibitor, MG132 (20 μM) was used for 20 h in the presence of CHX (Sigma). Then, at the indicated time points post-CHX treatment, cells were prepared for western blot assay and immunobands were quantified (see section below 'Western-blot analysis and antibodies' for details). The half-life values of 3xFLAGged proteins and Mcl-1 were calculated by nonlinear regression analysis using GRAPHPAD Prism software (San Diego, CA, USA).

Apoptosis induction and detection

COS-1 cells (transiently transfected with 3xFLAG-vectors) or WEHI7.2 cells (stably transfected with the various pSFFV-Neo vectors) were treated with 1 μM STS (Sigma-Aldrich) for 6 h. At this time point, COS-1 cells were harvested and lyzed in a buffer containing 25 mM Hepes, pH 7.5, 1% Triton X-100, 10 glycerol, 0.3 M NaCl, 1.5 mM $MgCl_2$, 1mM DTT, 2 mM EDTA, 2 mM EGTA, and protease inhibitor cocktail tablets (Roche). COS-1 apoptosis progression was monitored via western blotting analysis of PARP-1 cleavage, as a downstream target of activated Caspase-3 (see also Fig. S1). Alternatively, the death index of WEHI7.2 cells was determined by the difference between the Trypan blue positive fraction of STS-treated cells and the DMSO-treated cells: $(\text{Trypan bluepositive})_{STS}$ $-(\text{Tryphan blue positive})_{DMSO}$ [Countess Automated Cell Counter, Thermo Fisher Scientific, Waltham, MA, USA].

Western blot analysis and antibodies

COS-1 and WEHI7.2 cells were lyzed using the lysis buffer described above in 'FLAG-co-immunoprecipitation assay'. The protein concentration of samples was determined by Bradford assay (Sigma-Aldrich) using BSA as a standard. Proteins (10–20 μg) were separated by NuPAGE 4–12%

Bis/Tris SDS-polyacrylamide gels using MES/SDS-running buffer (Invitrogen) and transferred onto a polyvinylidene fluoride (PVDF) membrane. After blocking with TBS containing 0.1% Tween and 5% nonfat dry milk powder, the membrane was incubated overnight with the appropriate primary antibody (diluted in 0.1% Tween/TBS). Next, membranes were incubated for 1 h with a secondary horseradish peroxidase (HRP)-conjugated antibody (dilution 1 : 2000 in 0.1% Tween/TBS). Protein detection was performed with Pierce ECL western Blotting Substrate (Thermo Fisher Scientific; p/a Perbio Science BVBA, Erembodegem, Belgium). Bands quantification was performed with IMAGEJ software (rsbweb.nih.gov/ij/).

In this study, we used the following primary antibodies: mouse monoclonal anti-FLAG M2-Peroxidase (HRP; 1 : 5000; Sigma-Aldrich); rabbit polyclonal anti-PARP-1 (1 : 1000, Alexis-Enzo Life Sciences, Farmingdale, NY, USA); mouse monoclonal anti-β-Actin (1 : 10 000; Sigma-Aldrich); mouse monoclonal anti-Bcl-2 (C2; 1 : 1000; Santa Cruz Biotechnology, Santa Cruz, CA, USA); rabbit anti-Mcl-1 Antibody (1 : 1000, S-19; Santa Cruz); penta-His HRP conjugate (1 : 1000; Qiagen, Hilden, Germany); rabbit polyclonal anti-Bax (1 : 1000, N-20; Santa Cruz); Monoclonal Anti-Vinculin (1 : 1000; Sigma-Aldrich); Monoclonal Anti-GAPDH antibody (1 : 10 000; Sigma-Aldrich).

Fura-2-Ca^{2+} imaging

COS-1 cells (2.5×10^5 cell·mL^{-1}) or WEHI7.2 cells (4×10^5 cells per well in poly-L-lysine–coated 96-well plates) were loaded with Fura-2-AM (5 μM; Biotium, Inc., Hayward, CA, USA) in modified Krebs buffer (135 mM NaCl, 5.9 mM KCl, 1.2 mM $MgCl_2$, 11.6 mM Hepes, pH 7.3, 11.5 mM glucose and 1.5 mM $CaCl_2$) for 30 min, followed by de-esterification for 30 min. To buffer all extracellular free Ca^{2+}, 5 mM BAPTA (Invitrogen) or 3 mM EGTA were added before each measurement in COS-1 cells or WEHI7.2 cells, respectively. Ca^{2+} rises in response to the physiological agonists ATP (1 μM) or to submaximal concentration of anti-CD3 antibody (10 μg·mL^{-1}, [33], BD Biosciences, San Jose, CA, USA) were measured ratiometrically (excitation at 340 nm/380 nm, emission detection at 510 nm) using Zeiss Axio Observer Z1 Inverted Microscope equipped with a 20× air objective and an high-speed digital camera (Axiocam Hsm, Zeiss, Jena, Germany), or using a FlexStation 3 microplate reader (Molecular Devices, Sunnyvale, CA, USA). Intracellular cytoplasmic Ca^{2+} concentrations were calculated as described in [18] for microscope recordings or as in [73] for microplate reader recordings. Traces were normalized to baseline levels with Excel software (Microsoft Office, Redmond, WA, USA) and for each experiment the average peak value ($\Delta[Ca^{2+}]$cyt) was determined. COS-1 cells were also challenged with TG (5 μM) to assess ER Ca^{2+}-store content and the changes in the Ca^{2+} concentration ($\Delta[Ca^{2+}]$) were quantified as area under the curve (AUC).

XBP-1 mRNA splicing assay

Twelve hours or 48 h after COS-1 transfection, RNA was extracted using a high pure RNA isolation kit (Roche) according to the manufacturer's directions. cDNA was obtained using a high capacity cDNA reverse transcription kit (Applied Biosystems, Foster City, CA, USA) following the guidelines suggested by the manufacturer. The presence of XBP-1 and its spliced product was assessed by PCR utilizing the following primers: forward 5′-GTTAAGACAGC GCCTGGGGATGG-3′ and reverse 5′-GGGAATCCATG GGGAGAT GTTCTG-3′. Thermocycler conditions were as follows: 94 °C for 4 min, 24 cycles of 94 °C for 30 s, 58 °C for 45 s, and 72 °C for 45 s, with a final extension at 72 °C for 10 min. PCR products were run on a 1% agarose gel (Life Technologies, Carlsbad, CA, USA) containing ethidium bromide (Sigma-Aldrich). A Gene Flash system (Westburg, Leusden, Netherlands) was used for visualization.

Data and statistical analysis

Data are expressed as means ± SEM. Statistically significant differences were considered at $P < 0.05$ (single symbols), $P < 0.01$ (double symbols) and $P < 0.001$ (triple symbols) after using GRAPHPAD Prism 6 to perform a two-tailed paired Student's t test. However, when comparing three or more different conditions, we used a one-way ANOVA or a Friedman test, with or without Bonferroni adjustment. Each figure legend details the specific test used for each experiment with relative stat results.

Acknowledgements

The authors thank Anja Florizoone and Marina Crabbe for the excellent technical help. The authors are grateful to Dr. Clark Distelhorst (Case Western Reserve University, Cleveland, OH) and Dr. Santeri Kiviluoto (Yale school of medicine, New Haven, Connecticut) for providing WEHI7.2 cells overexpressing Bcl-2 and for technical support with XBP-1 splicing assay, respectively. The authors also thank all laboratory members for the fruitful discussions. This study was supported by grants from the Research Foundation-Flanders (FWO grants 6.057.12 to GB, JBP, HDS, G.0819.13 to GB, HDS, G.0C91.14 to GB, JBP), by the Research Council of the KU Leuven (OT grant 14/101 to GB) and by the Interuniversity Attraction Poles Program (Belgian Science Policy; IAP-P7/13 to JBP, GB). HI is a recipient of a post doctoral fellowship of the FWO. GM and EV are recipients of a postdoctoral fellowship of the FWO.

Author contributions

GM and GB designed the study with additional inputs from JBP and HDS. GM, RLR, SK, HI, and KW performed the research and analyzed the data. GM and GB drafted the manuscript. GM integrated all the data into the figures. JBP, HDS, MDM, EV, DDB, and AT revised critically the article for important intellectual content. All authors interpreted the results.

References

1 Hardwick JM & Soane L (2013) Multiple functions of BCL-2 family proteins. *Cold Spring Harb Perspect Biol* **5**.

2 Vervliet T, Parys JB & Bultynck G (2016) Bcl-2 proteins and calcium signaling: complexity beneath the surface. *Oncogene* **35**, 5079–5092.

3 Gillies LA & Kuwana T (2014) Apoptosis regulation at the mitochondrial outer membrane. *J Cell Biochem* **115**, 632–640.

4 Kvansakul M, Yang H, Fairlie WD, Czabotar PE, Fischer SF, Perugini MA, Huang DC & Colman PM (2008) Vaccinia virus anti-apoptotic F1L is a novel Bcl-2-like domain-swapped dimer that binds a highly selective subset of BH3-containing death ligands. *Cell Death Differ* **15**, 1564–1571.

5 Siddiqui WA, Ahad A & Ahsan H (2015) The mystery of BCL2 family: Bcl-2 proteins and apoptosis: an update. *Arch Toxicol* **89**, 289–317.

6 Zha H & Reed JC (1997) Heterodimerization-independent functions of cell death regulatory proteins Bax and Bcl-2 in yeast and mammalian cells. *J Biol Chem* **272**, 31482–31488.

7 Cantara S, Donnini S, Giachetti A, Thorpe PE & Ziche M (2004) Exogenous BH4/Bcl-2 peptide reverts coronary endothelial cell apoptosis induced by oxidative stress. *J Vasc Res* **41**, 202–207.

8 McDunn JE, Muenzer JT, Dunne B, Zhou A, Yuan K, Hoekzema A, Hilliard C, Chang KC, Davis CG, McDonough J *et al.* (2009) An anti-apoptotic peptide improves survival in lethal total body irradiation. *Biochem Biophys Res Commun* **382**, 657–662.

9 Barclay LA, Wales TE, Garner TP, Wachter F, Lee S, Guerra RM, Stewart ML, Braun CR, Bird GH, Gavathiotis E *et al.* (2015) Inhibition of Pro-apoptotic BAX by a noncanonical interaction mechanism. *Mol Cell* **57**, 873–886.

10 Monaco G, Decrock E, Nuyts K, Wagner LE, Luyten T, Strelkov SV, Missiaen L, De Borggraeve WM, Leybaert L, Yule DI *et al.* (2013) Alpha-helical destabilization of the Bcl-2-BH4-domain peptide abolishes its ability to inhibit the IP3 receptor. *PLoS ONE* **8**, e73386.

11 Shimizu S, Konishi A, Kodama T & Tsujimoto Y (2000) BH4 domain of antiapoptotic Bcl-2 family members closes voltage-dependent anion channel and inhibits apoptotic mitochondrial changes and cell death. *Proc Natl Acad Sci USA* **97**, 3100–3105.

12 Hanada M, Aimé-Sempé C, Sato T & Reed JC (1995) Structure-function analysis of Bcl-2 protein. Identification of conserved domains important for homodimerization with Bcl-2 and heterodimerization with Bax. *J Biol Chem* **270**, 11962–11969.

13 Huang DC, Adams JM & Cory S (1998) The conserved N-terminal BH4 domain of Bcl-2 homologues is essential for inhibition of apoptosis and interaction with CED-4. *EMBO J* **17**, 1029–1039.

14 Cheng EH, Kirsch DG, Clem RJ, Ravi R, Kastan MB, Bedi A, Ueno K & Hardwick JM (1997) Conversion of Bcl-2 to a Bax-like death effector by caspases. *Science* **278**, 1966–1968.

15 Kirsch DG, Doseff A, Chau BN, Lim DS, de Souza-Pinto NC, Hansford R, Kastan MB, Lazebnik YA & Hardwick JM (1999) Caspase-3-dependent cleavage of Bcl-2 promotes release of cytochrome c. *J Biol Chem* **274**, 21155–21161.

16 Hirotani M, Zhang Y, Fujita N, Naito M & Tsuruo T (1999) NH2-terminal BH4 domain of Bcl-2 is functional for heterodimerization with Bax and inhibition of apoptosis. *J Biol Chem* **274**, 20415–20420.

17 Rong Y-P, Bultynck G, Aromolaran AS, Zhong F, Parys JB, De Smedt H, Mignery GA, Roderick HL, Bootman MD & Distelhorst CW (2009) The BH4 domain of Bcl-2 inhibits ER calcium release and apoptosis by binding the regulatory and coupling domain of the IP3 receptor. *Proc Natl Acad Sci USA* **106**, 14397–14402.

18 Monaco G, Decrock E, Akl H, Ponsaerts R, Vervliet T, Luyten T, De Maeyer M, Missiaen L, Distelhorst CW, De Smedt H *et al.* (2012) Selective regulation of IP_3-receptor-mediated Ca^{2+} signaling and apoptosis by the BH4 domain of Bcl-2 versus Bcl-Xl. *Cell Death Differ* **19**, 295–309.

19 Lee LC, Hunter JJ, Mujeeb A, Turck C & Parslow TG (1996) Evidence for alpha-helical conformation of an essential N-terminal region in the human Bcl2 protein. *J Biol Chem* **271**, 23284–23288.

20 de Moissac D, Zheng H & Kirshenbaum LA (1999) Linkage of the BH4 domain of Bcl-2 and the nuclear factor kappaB signaling pathway for suppression of apoptosis. *J Biol Chem* **274**, 29505–29509.

21 Trisciuoglio D, Gabellini C, Desideri M, Ragazzoni Y, De Luca T, Ziparo E & Del Bufalo D (2011) Involvement of BH4 domain of bcl-2 in the regulation of HIF-1-mediated VEGF expression in hypoxic tumor cells. *Cell Death Differ* **18**, 1024–1035.

22 Ding J, Zhang Z, Roberts GJ, Falcone M, Miao Y, Shao Y, Zhang XC, Andrews DW & Lin J (2010) Bcl-2

and Bax interact via the BH1-3 groove-BH3 motif interface and a novel interface involving the BH4 motif. *J Biol Chem* **285**, 28749–28763.
23 Rong Y-P, Barr P, Yee VC & Distelhorst CW (2009) Targeting Bcl-2 based on the interaction of its BH4 domain with the inositol 1,4,5-trisphosphate receptor. *Biochim Biophys Acta* **1793**, 971–978.
24 Hecht M, Bromberg Y & Rost B (2015) Better prediction of functional effects for sequence variants. *BMC Genom* **16** (Suppl 8), S1.
25 Choi Y & Chan AP (2015) PROVEAN web server: a tool to predict the functional effect of amino acid substitutions and indels. *Bioinformatics* **31**, 2745–2747.
26 Li B, Krishnan VG, Mort ME, Xin F, Kamati KK, Cooper DN, Mooney SD & Radivojac P (2009) Automated inference of molecular mechanisms of disease from amino acid substitutions. *Bioinformatics* **25**, 2744–2750.
27 Capriotti E, Calabrese R & Casadio R (2006) Predicting the insurgence of human genetic diseases associated to single point protein mutations with support vector machines and evolutionary information. *Bioinformatics* **22**, 2729–2734.
28 Vervliet T, Lemmens I, Welkenhuyzen K, Tavernier J, Parys JB & Bultynck G (2015) Regulation of the ryanodine receptor by anti-apoptotic Bcl-2 is independent of its BH3-domain-binding properties. *Biochem Biophys Res Commun* **463**, 174–179.
29 Petros AM, Olejniczak ET & Fesik SW (2004) Structural biology of the Bcl-2 family of proteins. *Biochim Biophys Acta* **1644**, 83–94.
30 Yin XM, Oltvai ZN & Korsmeyer SJ (1994) BH1 and BH2 domains of Bcl-2 are required for inhibition of apoptosis and heterodimerization with Bax. *Nature* **369**, 321–323.
31 Joseph SK, Pierson S & Samanta S (1995) Trypsin digestion of the inositol trisphosphate receptor: implications for the conformation and domain organization of the protein. *Biochem J* **307** (Pt 3), 859–865.
32 Rong Y-P, Aromolaran AS, Bultynck G, Zhong F, Li X, McColl K, Matsuyama S, Herlitze S, Roderick HL, Bootman MD *et al.* (2008) Targeting Bcl-2-IP3 receptor interaction to reverse Bcl-2′s inhibition of apoptotic calcium signals. *Mol Cell* **31**, 255–265.
33 Zhong F, Davis MC, McColl KS & Distelhorst CW (2006) Bcl-2 differentially regulates Ca2 + signals according to the strength of T cell receptor activation. *J Cell Biol* **172**, 127–137.
34 Distelhorst CW & Bootman MD (2011) Bcl-2 interaction with the inositol 1,4,5-trisphosphate receptor: role in Ca(2 +) signaling and disease. *Cell Calcium* **50**, 234–241.
35 Yang J & Zhang Y (2015) Protein structure and function prediction using I-TASSER. *Curr Protoc Bioinformatics* **52**, 5.8.1–5.815.
36 Kelley LA, Mezulis S, Yates CM, Wass MN & Sternberg MJE (2015) The Phyre2 web portal for protein modeling, prediction and analysis. *Nat Protoc* **10**, 845–858.
37 Schymkowitz J, Borg J, Stricher F, Nys R, Rousseau F & Serrano L (2005) The FoldX web server: an online force field. *Nucleic Acids Res* **33**, W382–W388.
38 Yin S, Ding F & Dokholyan NV (2007) Eris: an automated estimator of protein stability. *Nat Methods* **4**, 466–467.
39 Benedix A, Becker CM, de Groot BL, Caflisch A & Böckmann RA (2009) Predicting free energy changes using structural ensembles. *Nat Methods* **6**, 3–4.
40 Capriotti E, Fariselli P & Casadio R (2005) I-Mutant2.0: predicting stability changes upon mutation from the protein sequence or structure. *Nucleic Acids Res* **33**, W306–W310.
41 Pires DEV, Ascher DB & Blundell TL (2014) DUET: a server for predicting effects of mutations on protein stability using an integrated computational approach. *Nucleic Acids Res* **42**, W314–W319.
42 Daniel RM, Cowan DA, Morgan HW & Curran MP (1982) A correlation between protein thermostability and resistance to proteolysis. *Biochem J* **207**, 641–644.
43 Parsell DA & Sauer RT (1989) The structural stability of a protein is an important determinant of its proteolytic susceptibility in Escherichia coli. *J Biol Chem* **264**, 7590–7595.
44 Baneyx F & Mujacic M (2004) Recombinant protein folding and misfolding in Escherichia coli. *Nat Biotechnol* **22**, 1399–1408.
45 Khan KH (2013) Gene expression in Mammalian cells and its applications. *Adv Pharm Bull* **3**, 257–263.
46 Nijhawan D, Fang M, Traer E, Zhong Q, Gao W, Du F & Wang X (2003) Elimination of Mcl-1 is required for the initiation of apoptosis following ultraviolet irradiation. *Genes Dev* **17**, 1475–1486.
47 Maurer U, Charvet C, Wagman AS, Dejardin E & Green DR (2006) Glycogen synthase kinase-3 regulates mitochondrial outer membrane permeabilization and apoptosis by destabilization of MCL-1. *Mol Cell* **21**, 749–760.
48 Hetz C, Martinon F, Rodriguez D & Glimcher LH (2011) The unfolded protein response: integrating stress signals through the stress sensor IRE1α. *Physiol Rev* **91**, 1219–1243.
49 van Schadewijk A, van't Wout EFA, Stolk J & Hiemstra PS (2012) A quantitative method for detection of spliced X-box binding protein-1 (XBP1) mRNA as a measure of endoplasmic reticulum (ER) stress. *Cell Stress Chaperones* **17**, 275–279.
50 Rutkowski DT & Kaufman RJ (2004) A trip to the ER: coping with stress. *Trends Cell Biol* **14**, 20–28.

51 Thomas LW, Lam C & Edwards SW (2010) Mcl-1; the molecular regulation of protein function. *FEBS Lett* **584**, 2981–2989.
52 Sugioka R, Shimizu S, Funatsu T, Tamagawa H, Sawa Y, Kawakami T & Tsujimoto Y (2003) BH4-domain peptide from Bcl-xL exerts anti-apoptotic activity *in vivo*. *Oncogene* **22**, 8432–8440.
53 Ono M, Sawa Y, Ryugo M, Alechine AN, Shimizu S, Sugioka R, Tsujimoto Y & Matsuda H (2005) BH4 peptide derivative from Bcl-xL attenuates ischemia/reperfusion injury thorough anti-apoptotic mechanism in rat hearts. *Eur J Cardiothorac Surg* **27**, 117–121.
54 Soto P & Smith LC (2009) BH4 peptide derived from Bcl-xL and Bax-inhibitor peptide suppresses apoptotic mitochondrial changes in heat stressed bovine oocytes. *Mol Reprod Dev* **76**, 637–646.
55 Mincheva-Tasheva S, Obis E, Tamarit J & Ros J (2014) Apoptotic cell death and altered calcium homeostasis caused by frataxin depletion in dorsal root ganglia neurons can be prevented by BH4 domain of Bcl-xL protein. *Hum Mol Genet* **23**, 1829–1841.
56 Monaco G, Decrock E, Arbel N, van Vliet AR, La Rovere RM, De Smedt H, Parys JB, Agostinis P, Leybaert L, Shoshan-Barmatz V *et al.* (2015) The BH4 domain of anti-apoptotic Bcl-XL, but not that of the related Bcl-2, limits the voltage-dependent anion channel 1 (VDAC1)-mediated transfer of pro-apoptotic Ca2 + signals to mitochondria. *J Biol Chem* **290**, 9150–9161.
57 Trisciuoglio D, De Luca T, Desideri M, Passeri D, Gabellini C, Scarpino S, Liang C, Orlandi A & Del Bufalo D (2013) Removal of the BH4 domain from Bcl-2 protein triggers an autophagic process that impairs tumor growth. *Neoplasia* **15**, 315–327.
58 Williams A, Hayashi T, Wolozny D, Yin B, Su T-C, Betenbaugh MJ & Su T-P (2016) The non-apoptotic action of Bcl-xL: regulating Ca(2 +) signaling and bioenergetics at the ER-mitochondrion interface. *J Bioenerg Biomembr* **48**, 211–225.
59 Vervliet T, Decrock E, Molgó J, Sorrentino V, Missiaen L, Leybaert L, De Smedt H, Kasri NN, Parys JB & Bultynck G (2014) Bcl-2 binds to and inhibits ryanodine receptors. *J Cell Sci* **127**, 2782–2792.
60 Ahn T, Yun C-H, Kim H-R & Chae H-J (2010) Cardiolipin, phosphatidylserine, and BH4 domain of Bcl-2 family regulate Ca2 + /H+ antiporter activity of human Bax inhibitor-1. *Cell Calcium* **47**, 387–396.
61 Lin B, Kolluri SK, Lin F, Liu W, Han Y-H, Cao X, Dawson MI, Reed JC & Zhang X-K (2004) Conversion of Bcl-2 from protector to killer by interaction with nuclear orphan receptor Nur77/TR3. *Cell* **116**, 527–540.
62 Bromberg Y & Rost B (2009) Correlating protein function and stability through the analysis of single amino acid substitutions. *BMC Bioinformatics* **10** (Suppl 8), S8.
63 Teilum K, Olsen JG & Kragelund BB (2011) Protein stability, flexibility and function. *Biochim Biophys Acta* **1814**, 969–976.
64 Pace CN, Fu H, Fryar KL, Landua J, Trevino SR, Shirley BA, Hendricks MM, Iimura S, Gajiwala K, Scholtz JM *et al.* (2011) Contribution of hydrophobic interactions to protein stability. *J Mol Biol* **408**, 514–528.
65 Sandelin E (2004) On hydrophobicity and conformational specificity in proteins. *Biophys J* **86**, 23–30.
66 Rooswinkel RW, van de Kooij B, de Vries E, Paauwe M, Braster R, Verheij M & Borst J (2014) Antiapoptotic potency of Bcl-2 proteins primarily relies on their stability, not binding selectivity. *Blood* **123**, 2806–2815.
67 Han B, Park D, Li R, Xie M, Owonikoko TK, Zhang G, Sica GL, Ding C, Zhou J, Magis AT *et al.* (2015) Small-molecule Bcl2 BH4 antagonist for lung cancer therapy. *Cancer Cell* **27**, 852–863.
68 Schneider K & Bertolotti A (2015) Surviving protein quality control catastrophes–from cells to organisms. *J Cell Sci* **128**, 3861–3869.
69 Hetz C (2012) The unfolded protein response: controlling cell fate decisions under ER stress and beyond. *Nat Rev Mol Cell Biol* **13**, 89–102.
70 Rashid H-O, Yadav RK, Kim H-R & Chae H-J (2015) ER stress: autophagy induction, inhibition and selection. *Autophagy* **11**, 1956–1977.
71 Maiti R, Van Domselaar GH, Zhang H & Wishart DS (2004) SuperPose: a simple server for sophisticated structural superposition. *Nucleic Acids Res* **32**, W590–W594.
72 Chen R, Valencia I, Zhong F, McColl KS, Roderick HL, Bootman MD, Berridge MJ, Conway SJ, Holmes AB, Mignery GA *et al.* (2004) Bcl-2 functionally interacts with inositol 1,4,5-trisphosphate receptors to regulate calcium release from the ER in response to inositol 1,4,5-trisphosphate. *J Cell Biol* **166**, 193–203.
73 Decuypere J-P, Welkenhuyzen K, Luyten T, Ponsaerts R, Dewaele M, Molgó J, Agostinis P, Missiaen L, De Smedt H, Parys JB *et al.* (2011) Ins(1,4,5)P3 receptor-mediated Ca2 + signaling and autophagy induction are interrelated. *Autophagy* **7**, 1472–1489.
74 Souers AJ, Leverson JD, Boghaert ER, Ackler SL, Catron ND, Chen J, Dayton BD, Ding H, Enschede SH, Fairbrother WJ *et al.* (2013) ABT-199, a potent and selective BCL-2 inhibitor, achieves antitumor activity while sparing platelets. *Nat Med* **19**, 202–208.

Supporting information

Additional Supporting Information may be found online in the supporting information tab for this article:

Fig. S1. Values obtained from the immunoreactive quantification of cleaved over total PARP (complementing Fig. 2D,E).

Fig. S2. Detailed view of the wavelength scans (190–260 nm) coupled to temperature scans (15–85 °C; 5 °C step; 1 °C·min^{-1}; complementing Fig. 4E).